Optical Beam Steering using Optical Phased Array for LIDAR

MS (Research) Thesis

By

CHITTIPROLU SAI GANESH

Under the supervision of

PROF. MUKESH KUMAR

DEPARTMENT OF ELECTRICAL ENGINEERING
INDIAN INSTITUTE OF TECHNOLOGY INDORE
JUNE 2024

Optical Beam Steering using Optical Phased Array for LIDAR

A Thesis

Submitted in partial fulfillment of the requirements for the award of the degree of

Master of Science (Research)

by

CHITTIPROLU SAI GANESH

DEPARTMENT OF ELECTRICAL ENGINEERING

INDIAN INSTITUTE OF TECHNOLOGY INDORE

JUNE 2024

INDIAN INSTITUTE OF TECHNOLOGY INDORE

CANDIDATE'S DECLARATION

I hereby certify that the work which is being presented in the thesis entitled **Optical Beam Steering using Optical Phased Array for LIDAR** in the partial fulfillment of the requirements for the award of the degree of **Master of Science - Research** and submitted in the **Department of Electrical Engineering, Indian Institute of Technology Indore,** is an authentic record of my own work carried out during the time period from July 2022 to June 2024 under the supervision of Dr. Mukesh Kumar, Professor, Indian Institute of Technology Indore, Indore, India.

The matter presented in this thesis has not been submitted by me for the award of any other degree of this or any other institute.

Sai Ganesh 07/06/2025

Signature of the Student with Date

(Chittiprolu Sai Ganesh)

This is to certify that the above statement made by the candidate is correct to the best of my knowledge.

7/06/2025

Signature of the Supervisor of MS-R Thesis with Date

(Prof. Mukesh Kumar)

Chittiprolu Sai Ganesh has successfully given his MS - Research Oral Examination held on **DD/MM/YYYY**

Signature of Thesis Supervisor with date

Saptarshi Ghosh

Signature of Convener, DPGC with date

Signature of Chairperson, OEB with date

P. Sanjeeth (Acting HoD-EE)

Signature of Head of Department with date

This Thesis is Dedicated
to
Lord Krishna

ACKNOWLEDGEMENTS

I am immensely grateful to my MS Research thesis supervisor and mentor, Prof. Mukesh Kumar, for consistently encouraging and supporting me in both my research and personal growth. He is not only a good professor, but also a great human being. I will always remember the conversations I had with him, and look forward to more in the later part of my life.

My family has played an integral role in supporting my research work throughout my master's program. I am deeply grateful for their unwavering guidance, love, and sacrifices. Their faith in me has not only brought me this far but will continue to drive me to achieve even greater things. Whatever I am today, how I managed to balance my personal and professional life while undertaking this research, it's all because of my family. They have nurtured and supported me throughout my life, and I am forever indebted to them.

I deeply appreciate the OptoElectronic Nano Resarch Laboratory (ONRL) research group, especially Mr. Prem Babu, Ms. Nikita Mohanta, Mr. Santosh Kumar, Mr. Ashutosh Rajpoot, Mr. Rahul Dev Mishra, Mr. Suresh Pandey ,Ms. Swati Rajput, Mr. Sudhir Gill and Mr. Suman for their continuous support and guidance.

I want to express my sincere gratitude to my friends Shruti Ghodke, Ankit Patel, Radhe Shyam, Komal Gupta, Gulrez Khan, and Neeraj Nikhil. Their friendship and encouragement were invaluable during my time at the institute, and I will always cherish the memories we made together.

The memories I made here will always be a source of joy and inspiration.This institute has been more than just a place of learning, it has been a community that has nurtured my personal and professional development. I am thankful for the friendships formed, the lessons learned, and the memories created within these walls.

Chittiprolu Sai Ganesh

ABSTRACT

This study presents a comprehensive simulation-based investigation of a 1x16 channel optical phased array (OPA), highlighting the advantages of utilizing Si-ITO phase shifters over conventional Si-based devices. Through rigorous FDTD simulations, we achieved a compact OPA design with dimensions of 0.07 mm x 0.02 mm, demonstrating remarkable steering capabilities. The Si-ITO phase shifters enabled a wide lateral steering range of 56°, surpassing the performance of conventional phase shifters that would require significantly larger apertures to achieve similar results. Additionally, we achieved a 23° longitudinal steering range through wavelength tuning from 1.5 μm to 1.6 μm, with a divergence angle of 3.5° x 7.5°. The use of Si-ITO as a phase shifter, owing to its superior electro-optic effect, addresses the inherent limitations of traditional phase shifters, particularly their larger footprints. The chip-scale dimensions of ITO play a crucial role in achieving compact phase shifters, essential for high-density on-chip packaging. This advancement in Si-ITO technology holds significant promise for the development of compact, efficient, and high-performance OPAs for future on-chip optical communication systems.

Publications

1. **Chittiprolu Sai Ganesh**, Shikha Devi, Prem Babu, Nikita Mohanta, Santosh Kumar, and Mukesh Kumar "2D Optical Beam Steering using Phase-Tuning in Si-ITO based Optical Phased Arrays," **Optical and Quantum Electronics** (Under Review)

Contents

List of Figures

List of Abbreviations

GC	-	Grating Coupler
OPA	-	Optical Phased Array
EO	-	Electro-Optic
TO	-	Thermo-Optic
FWHM	-	Full Width Half Maximum
MMI	-	Multi-Mode Interference
ITO	-	Indium Tin Oxide
LIDAR	-	Light Detection and Ranging
neff	-	Effective Refractive Index
NIR	-	Near Infrared
PIC	-	Photonics Integrated Circuits
SiPho	-	Silicon Photonics
CMOS	-	Complementary Metal-Oxide Semiconductor
FOV	-	Field of view
TM Mode	-	Transverse Magnetic Mode
TE Mode	-	Transverse Electric Mode
DBR	-	Distributed Bragg Reflector
ITO	-	Indium Tin Oxide

Chapter 1

Introduction

This chapter provides an introduction to the various topics which are necessary in understanding the work carried out.

1.1 Integrated Photonics

The ever-growing demands for faster data transfer, reduced energy consumption, and increased processing power have highlighted the limitations of traditional semiconductor electronics. Modern applications, particularly data-intensive fields like artificial intelligence and machine learning, require real-time processing of massive datasets, a task that conventional electronics are struggling to keep pace with, Historically shrinking electronic components has led to advancements in speed, power efficiency, affordability, and size reduction. However, this approach is now approaching its inherent limits. Short-channel effects and fundamental speed and bandwidth constraints are impeding further progress across various scientific and technological disciplines. The expanding gap between processing capabilities and memory bandwidth, as evidenced by the modest 5-10 TDP-FLOP/Byte ratio of current high-performance processors, underscores the critical need for innovative solutions to significantly boost data transfer rates[1].

Electronic interconnects, hindered by latency and losses, pose a substantial obstacle to achieving electronic circuits operating above 10 GHz. Photonic devices, which utilize light as the information carrier, offer a potential way forward. Nevertheless, the size and complexity of conventional photonic components have, until recently, prevented their seamless integration with electronics on a single chip. The emergence of nanophotonics,a field dedi-

cated to manipulating light beyond its diffraction limit, has revolutionized this landscape. Photonic Integrated Circuits (PICs), as illustrated in Figure.1.1 , exemplify the successful integration of both passive and active photonic components onto a single substrate. Waveguides, acting as conduits for light, connect these components, enabling the development of compact and robust photonic devices. This integration not only enhances the performance and dependability of photonic functions but also significantly reduces the overall size, weight, and power consumption of these devices[2].

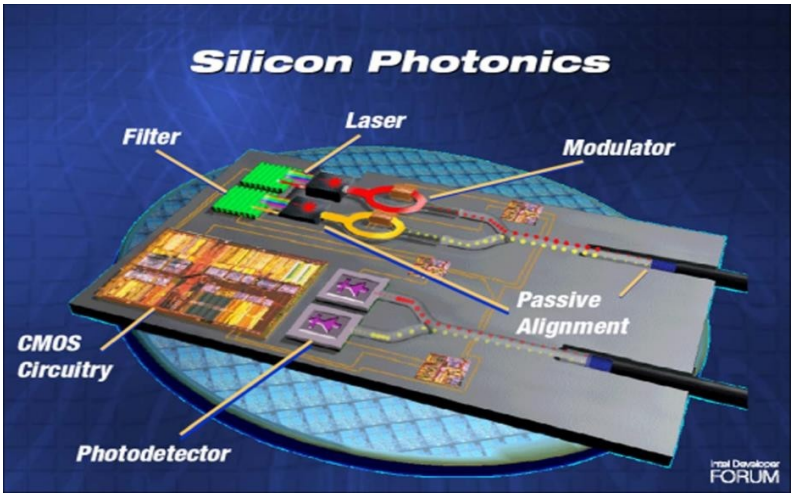

Figure 1.1: A Si photonic integrated circuit depicting the integration of photonic components with CMOS circuitry [3].

1.2 LIDAR

LiDAR, which stands for Light Detection and Ranging, is a remote sensing technology that utilizes laser light to measure distances from the sensor to a target. The basic components of a LiDAR system include a laser, a scanner, and a GPS receiver. The laser emits pulses of light towards the ground, and the scanner captures the light reflected back from various surfaces. By calculating the time it takes for the light to return to the sensor, the system can determine the distance to each point on the ground, creating a detailed three-dimensional map of the surface.The origins of LiDAR technology can be traced back to the early 1960s, when it was first developed for meteorological studies and atmospheric research. Since then, it has evolved significantly and found applications in various fields such as geography, forestry, environmental science, archaeology, and urban planning. LiDAR's ability to pene-

trate dense vegetation and provide high-resolution data makes it particularly valuable for mapping and analyzing forested areas, where traditional surveying methods may be less effective.One of the key advantages of LiDAR is its precision and accuracy. Modern LiDAR systems can generate point clouds with densities exceeding millions of points per square meter, allowing for the creation of highly detailed and accurate digital elevation models (DEMs). These models are essential for applications such as flood risk assessment, terrain analysis, and infrastructure planning. Additionally, LiDAR can operate effectively both day and night, as it relies on its own emitted light rather than ambient light conditions.

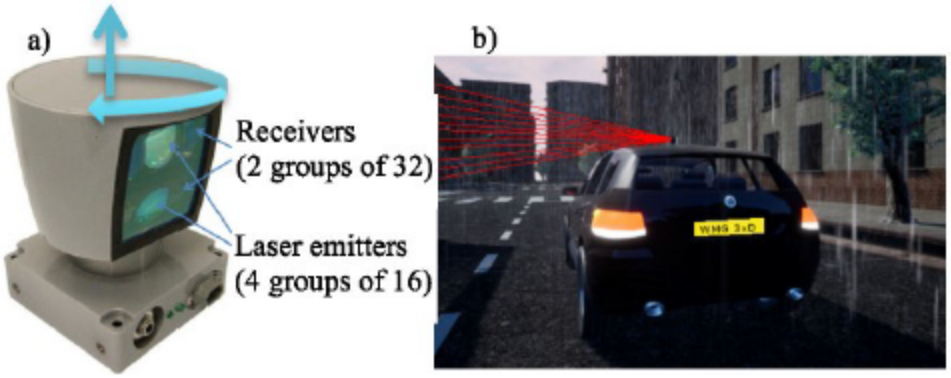

Figure 1.2: (a) Mechanical Rotating LiDAR, modified from [4] (b) 360° rotating LiDAR on a vehicle, red lines represent the vertical channels.

The integration of LiDAR with other remote sensing technologies, such as aerial photography and satellite imagery, further enhances its capabilities. This synergy allows for more comprehensive and accurate environmental monitoring and mapping, providing critical insights for decision-making and policy development. For example, combining LiDAR data with multispectral or hyperspectral imagery can improve the identification and classification of different land cover types, aiding in ecological and land management studies.Recent advancements in LiDAR technology have also led to the development of mobile and terrestrial LiDAR systems, which can be mounted on vehicles or tripod-mounted scanners for ground-based surveys. These systems are used for applications such as roadway mapping, construction site monitoring, and heritage conservation. The portability and flexibility of these systems enable rapid and detailed data collection in various environments, from urban landscapes to remote natural areas.Overall, LiDAR represents a significant leap forward in remote sensing, offering unparalleled accuracy and

detail in capturing the Earth's surface. Its versatility and precision continue to drive its adoption across various sectors, highlighting its importance in modern geographical and environmental studies.

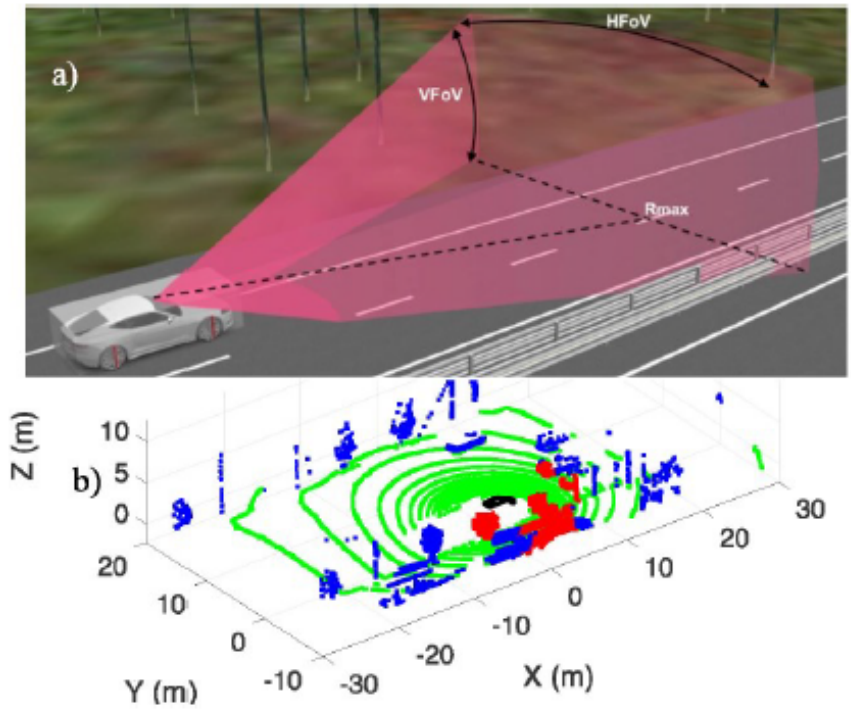

Figure 1.3: (a) Simplified representation of the spatial coverage by a generic environmental perception sensor, highlighted by the red volume in the figure. (b) Example of 3D LiDAR pointcloud, segmented, modified from [5].

1.3 Optical Beam Steering

Beam steering is a critical component in light detection and ranging (LIDAR) systems, with applications ranging from autonomous vehicles to advanced imaging devices[6][7]. Traditional mechanical beam steering methods, while effective, are no longer ideal for meeting the growing demand for compact, cost-effective, and high-resolution LIDAR systems due to their moving parts and complex calibration requirements[8][9].

Optical phased arrays (OPAs) have emerged as a promising alternative to their mechanical counterparts. OPAs offer reliable non-mechanical operation and a compact footprint, making them particularly attractive for in-

tegration into advanced imaging and scanning devices. In the realm of silicon (Si) photonics, various OPA designs have successfully demonstrated two-dimensional (2D) beam steering using complementary metal-oxide semiconductor (CMOS) processes[10][11].

1.4 Optical Phased Array Based LiDAR

Optical phased arrays (OPAs) are emerging as a promising solid-state technology for the development of fully integrated and cost-effective LiDAR sensors on silicon photonic (SiPho) chips.Inspired by the beam steering principles used in radio frequency (RF) systems, OPAs leverage phase delay and interference between multiple transmitting antennas to control the direction of electromagnetic beams.

A typical integrated silicon photonics OPA-LiDAR system comprises several key components: a light source, a beam splitter (often an MMI coupler or star coupler), phase shifters (either thermal or electro-optical), and the transmitting antennas themselves, commonly implemented as gratings or edge emitters as shown in Figure 1.4 . By introducing specific phase delays to the signals in the antennas, the emitted beam can be steered precisely towards a desired direction.

Notably, two-dimensional (2D) beam steering can be achieved with a simpler one-dimensional (1D) array of grating couplers (GCs). Wavelength tuning controls the longitudinal steering angle (θ), while the phase delay (Φ) between light injections in each GC governs the lateral steering angle (φ)[12][13]. This approach not only simplifies the design and fabrication of OPA-LiDAR systems but also maintains their beam steering capabilities.Within the realm of silicon photonics, phase shift manipulation—a key aspect of beam steering—has primarily been achieved through two distinct methods, both of which involve modifying the refractive index of the silicon waveguide, thereby altering the velocity of light propagating through it.

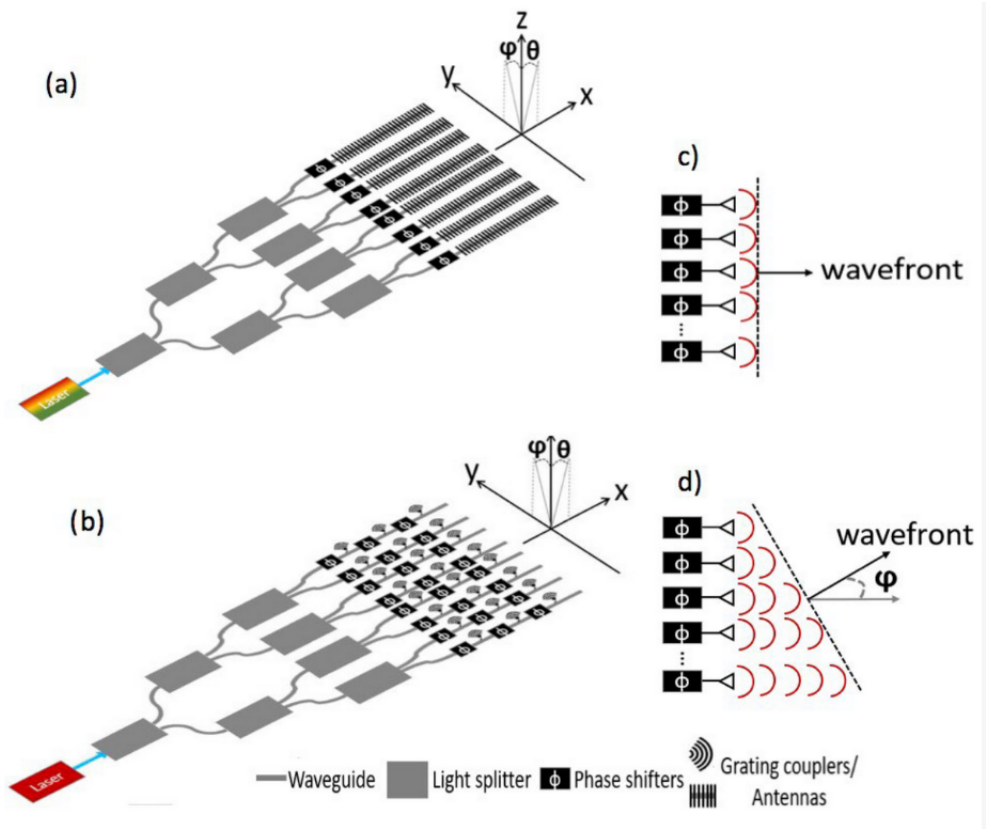

Figure 1.4: Schematic representations of the transmitting components and the emitted beam angles Φ AND θ in a 1D-OPA (a) and 2D-OPA (b) based LiDAR; the emitted waves with no phase delay between the emitting elements (c), and with phase delay (d), causing a rotation of the emitted wavefront along Φ [14] .

1.4.1 Thermo-optic (TO) effect

In silicon photonics, the refractive index of materials, particularly silicon, is temperature-dependent. For wavelengths around 1500 nm and temperatures near 295K, the refractive index of silicon (nSi) changes at a rate of

$$dnSi/dT = 1.87[*10^{-}4K^{-}1] \tag{1.1}$$

This property allows for thermal manipulation of the refractive index and consequently,the phase of light propagating through silicon waveguides. Figure 1.5 (a) shows a common method to increase the temperature of silicon waveguides involves utilizing the heat generated by a metal layer deposited on top of the upper cladding[15][16]. When a voltage is applied to this metal layer, the

Joule effect causes it to heat up, thereby increasing the temperature of the underlying silicon waveguide. This temperature change modifies the refractive index (nSi), introducing a phase delay compared to an unheated waveguide of the same length. A key advantage of these metal-heater-based phase shifters is their minimal impact on signal loss. However, they generally operate at lower speeds compared to other phase shifting technologies.

1.4.2 Electro-optic (EO) effect

Alternatively, the refractive index of silicon (nSi) can be modified through charge injection, achieved by creating and activating a p-i-n structure across the cross-section of a rib waveguide. This involves adding p and n dopants to the lateral sides of the waveguide,as shown in Figure 1.5 (b)[17]. Similar to the thermo-optic effect, the resulting change in refractive index introduces a phase delay compared to a non-doped or unactuated waveguide. This charge-injection method enables high-speed beam steering, with switching speeds in the nanosecond range. However, the presence of dopants increases waveguide losses, and the design becomes more intricate. Nevertheless, these electro-optic (EO) p-i-n phase shifters offer lower power consumption compared to thermo-optic (TO) phase shifters. While EO phase shifters provide faster operation than their TO counterparts, they do exhibit variable insertion loss, which is a trade-off to consider in system design.

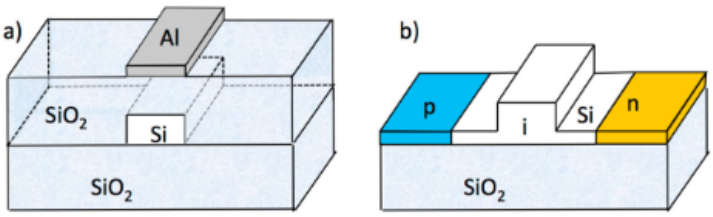

Figure 1.5: Schematic representation (not at scale) of the structure cross-section of (a) a TO phase shifter with Silicon strip waveguide, SiO2 lower and upper cladding, and heater metal layer (Aluminum or other metals compatible with CMOS thin layer deposition); (b) EO phase shifter with Silicon rib waveguide and doped (p and n) waveguide sides, SiO2 lower cladding; upper cladding not represented [18].

1.5 Optical Phased Array parameters

Optical phased arrays (OPAs) consist of an array of antennas or emitting components engineered to optimize the emission and steering of near-infrared (NIR) light. Several design parameters can be adjusted to enhance OPA performance, including maximizing steering range in both axes, improving beam directionality, suppressing unwanted side lobes, reducing crosstalk between elements, and increasing emitted power.

1.5.1 Array size (M x N)

The total number of elements within an optical phased array (OPA) is determined by the product of elements along the longitudinal axis (M) and the lateral axis (N), represented as M x N. This product signifies the total number of signals combined to achieve beam steering in the far field. A configuration with either M or N equaling 1 (e.g., 1 x 16) represents a one-dimensional (1D) array, typically used for beam steering along the lateral direction (ϕ).

1.5.2 Element spacing(d)

This represents the distance between two adjacent antenna elements.Combined with the array size above gives an approximation of the total antenna footprint.

1.5.3 Wavelength (λ)

The central wavelength (λ_0) of a grating coupler (GC) is the specific wavelength for which it is optimized. In some one-dimensional (1D) optical phased arrays (OPAs), beam steering along the longitudinal direction (θ) is achieved by varying the wavelength of the light injected into the antennas within a range ($\Delta\lambda$) around this central wavelength. This wavelength tuning mechanism enables dynamic control of the beam's direction in the longitudinal plane.

1.5.4 Lateral steering range (ϕ_{max})

it represents the lateral FoV. It can be calculated using below equation, where ϕ is the uniform phase difference between the signals emitted by the GCs.

$$sin\phi_{max} = \frac{\lambda_0\ \phi}{2\Pi \mathrm{d}} \tag{1.2}$$

In optical phased arrays (OPAs), as in radio wave OPA theory, the spacing (d) between adjacent antennas plays a crucial role in preventing the formation of undesirable grating side lobes, which are lateral emissions that detract from the main beam. To mitigate these side lobes, the spacing should ideally be smaller than half the operating wavelength

$$d < \frac{\lambda_0}{2} \tag{1.3}$$

However, this close proximity between antennas increases design complexity, as it necessitates careful consideration and minimization of crosstalk to maintain signal integrity.

1.5.5 Lateral beam width ($\Delta_{\phi FWHM}$)

The lateral beam width, representing the angular spread of the beam in the lateral direction,is a critical factor in optical phased array (OPA) design. A narrower beam width indicates higher directivity, which is often desirable. This beam width is influenced by the OPA's aperture size, determined by the number of elements (N) and their spacing (d). While increasing the aperture size generally narrows the beam, it can also lead to a trade-off: if the number of elements remains constant, the spacing between them increases, potentially reducing the lateral field of view (FOV).Conversely, decreasing the spacing between elements can introduce crosstalk, leading to power losses and decreased efficiency. Achieving a highly directional beam is essential for improving the lateral resolution of the sensor, especially at medium to long ranges. For instance, an angular resolution of around 0.1° is necessary to distinguish potential hazards and vulnerable road users, such as pedestrians, at distances up to 200 meters. To achieve this at a wavelength of 1550 nm, an aperture size of approximately 1.13 mm is required. One strategy to maintain a narrow beam while keeping the OPA design compact is to employ arrays with a non-uniform distribution of grating couplers (GCs). This approach allows for a wide steering range while suppressing undesirable grating side lobes, striking a balance between beam quality and device size.

$$\Delta_{\phi FWHM} = \frac{0.886\lambda_0}{\mathrm{Ndcos}\phi} \tag{1.4}$$

1.5.6 Longitudinal steering range (θ_{max})

The longitudinal field of view (FOV) in an optical phased array can be adjusted by altering the wavelength of light injected into the antennas. The

resulting emission angle (θ) can be calculated using the following equation.

$$sin\theta_{max} = \frac{\Lambda\text{neff-}\lambda_0}{\text{nclad}} \tag{1.5}$$

WhereΛ is the grating period neff is the effective refractive index of the waveguide at the central wavelength λ_0 nclad is the refractive index of the cladding material surrounding the silicon waveguide core.It's important to note that the effective refractive index (neff) is influenced by both temperature and wavelength, which can be leveraged for precise control over the longitudinal FOV.

1.5.7 Longitudinal beam width ($\Delta_{\theta FWHM}$)

Similar to the lateral beam width, the longitudinal beam width indicates the angular spread of the beam in the longitudinal direction. If beam steering in this direction is achieved by combining signals from multiple elements along the longitudinal axis, the beam width can be calculated by adapting the equation used for lateral beam width. However, if beam steering is accomplished through other means, such as wavelength tuning, the beam width will depend on factors like the grating structure, its length, and the chosen wavelength.

1.6 Current design challenges

1.6.1 Silicon Versus Silicon Nitride

Integrated optical waveguides operating in the near-infrared range can be fabricated using either silicon (Si) or silicon nitride (SiN) cores,both of which are compatible with standard foundry processes[19][20][21]. Both materials have been successfully employed in OPA-based LiDAR systems, demonstrating competitive performance.SiN offers broader wavelength transparency, extending to shorter wavelengths including 905 nm. This compatibility with existing 905 nm technology and components simplifies the development of solid-state LiDARs. Furthermore, SiN waveguides exhibit a higher power handling capacity compared to their Si counterparts. While foundry-compatible Si waveguides (typically 220 nm thick) operate linearly with power levels up to a few hundred milliwatts, SiN waveguides can tolerate higher powers before nonlinear effects become significant.Conversely, Si-based waveguides offer advantages in terms of footprint size. They can accommodate smaller dimensions and tighter bending radii (as small as 5 μm) without incurring substantial propagation losses. In contrast, SiN waveguides require larger

bend radii, exceeding 20 μm.Phase-shifting mechanisms also differ between the two materials. Si waveguides support both electro-optic (EO) and thermo-optic (TO) effects, while SiN exhibits a TO efficiency approximately one order of magnitude lower than Si. However, recent research has explored customizable photonics processes that combine Si and SiN elements to achieve optimized beam steering, leveraging the strengths of both materials.

1.6.2 Grating Coupler Design

Grating couplers (GCs) are essential components in silicon photonics (SiPho), serving as the interface between the on-chip waveguide and free-space light for applications like LiDAR beam generation.Various GC designs exist, aiming to minimize losses and maximize light emission efficiency. Side-modulated gratings and etched gratings (shallow or deep) are two common waveguide-based GC designs, characterized by alternating waveguide width or height, respectively[22]. Alternatively, compact GCs with strong perturbations, such as fully etched gratings, show promise for efficient light coupling. Moreover, sub-wavelength gratings (SWGs) and multi-box SWGs offer enhanced performance due to low-loss light propagation and increased evanescent fields. By carefully tuning grating parameters, optimized GCs for LiDAR applications can be achieved. However, grating structures are susceptible to fabrication variability, which can impact their performance. Additionally, some designs may not be compatible with CMOS processes due to the requirement for very small features. This fabrication variability poses a significant challenge for SiPho technology, particularly in meeting the stringent reliability and robustness standards of the automotive industry. Addressing these challenges is crucial for advancing on-chip light steering capabilities.

A key challenge in optimizing grating couplers (GCs) for optical phased arrays lies in achieving both long antenna lengths for enhanced beam directionality and uniform emission along the grating. Longer GCs offer a narrower longitudinal beam width ($\Delta_{\theta FWHM}$), improving the beam's focus and directionality. However, maintaining a uniform perturbation strength across a longer GC often results in decaying emission along the grating length, leading to reduced efficiency and beam quality.Apodized gratings, with strategically tailored perturbation strength along the propagation direction, have been employed to address this issue and achieve enhanced, uniform emission. By optimizing the effective aperture size of the GC, this approach can maximize both OPA gain and beam width.Additionally, beam uniformity is influenced by light emitted towards the chip substrate and subsequently reflected back upwards. To mitigate these reflections and further enhance beam quality, specialized GC designs incorporating multiple emitting layers or buried reflectors

have been proposed. These approaches aim to channel the emitted light more efficiently, improving the overall performance of the OPA system.

To increase the lateral field of view (FOV) in optical phased arrays (OPAs), reducing grating side lobes is crucial. In radio frequency (RF) systems, uniformly spaced antenna arrays with element spacing (d) smaller than half the operating wavelength,effectively suppress grating side lobes, allowing the main lobe to sweep the entire FOV. However in integrated photonic devices, maintaining this spacing while minimizing unwanted coupling between long parallel waveguides is challenging.Several design approaches can mitigate side lobes. Non-uniform and or aperiodic arrays have shown promise in side lobe suppression. However, if element spacing exceeds half the operating wavelength this approach increases device footprint without increasing the number of emitting elements.

1.6.3 OPA and Thermal Management

Integrating a light source onto silicon-on-insulator (SOI) chips remains a formidable challenge in the pursuit of fully integrated silicon photonic (SiPho) LiDAR systems. While existing solutions show promise, they are not yet mature enough for widespread commercial adoption, driving ongoing research to develop a more efficient and cost-effective approach.

Despite this challenge, significant advancements have been made in demonstrating optical beam steering and on-chip light source integration using various technologies. Hybrid III/V silicon technology, InP technology, and rare-earth-doped glass sources have all been explored, each with its unique advantages and drawbacks. Early demonstrations of 1D beam steering with integrated lasers have paved the way for more complex 2D beam steering systems, utilizing multiple lasers or innovative InP-based photonic integrated circuits[23][24].

The performance of OPA-LiDAR systems is intrinsically linked to three critical laser parameters: tunability, spectral linewidth, and emitted power. Tunability is especially important for 1D grating coupler arrays, where longitudinal steering (θ) is controlled by adjusting the laser wavelength. A high degree of tunability allows for finer control over the beam direction and, consequently, improved resolution. Spectral linewidth, representing the width of the laser's spectral density, directly impacts the system's resolution in both emission directions, along with the spatial beam widths. Lastly, high emitted laser power, combined with low-loss photonic circuitry, is paramount for maximizing the LiDAR's range and detection capabilities.

Emerging approaches, such as the monolithic integration of electronically steerable silicon photonic OPAs with rare-earth-doped lasers, hold great po-

tential for achieving the required power budgets for practical OPA-LiDAR systems. The continuous development of novel materials, fabrication techniques, and integration strategies will be key to overcoming the remaining challenges and realizing the full potential of integrated SiPho LiDAR technology.

Recent research has increasingly focused on heterogeneously integrated tunable laser sources, driven by their potential applications in various fields, including integrated LiDAR systems.A key method for achieving wavelength tuning in these laser sources involves the utilization of microring resonators configured in a Vernier architecture. This approach allows for precise and dynamic control over the emitted wavelength, which is a critical parameter for beam steering in LiDAR applications. The integration of tunable lasers with other photonic components on a single chip promises to further advance the development of compact, high-performance LiDAR systems for a wide range of applications.

1.6.4 Integration With Driving Electronics

A major challenge in silicon photonics (SiPho) technology is the integration of photonic circuitry with driving electronics. This integration can be achieved through either heterogeneous or monolithic approaches, both of which have implications for OPA-LiDAR development, where electrical signals are essential for both driving the system and receiving sensor output.

Monolithic integration, which involves combining electronics and photonics on a single chip, offers a compact and potentially cost-effective solution. However, CMOS design rules impose constraints on the photonic circuit design, ultimately impacting the OPA's performance. Notably, a scalable architecture for SiPho optical beam steering, monolithically integrated on the same wafer with a 180 nm CMOS driving circuit, has been demonstrated. Additionally, a compact design featuring both the integrated OPA and beam steering photonics circuit (2.08 mm^2) and its driving electronics (1.7 mm^2) has been realized using SOI and 65-nm CMOS processes, respectively.

In contrast, heterogeneous integration allows for independent optimization of CMOS and photonic processes, offering greater design flexibility. A promising approach for seamless heterogeneous integration involves utilizing 3D integration platforms. This method enables separate optimization of the two processes before combining them, for instance, through oxide bonding. The resulting integration offers the potential for enhanced performance and functionality in OPA-LiDAR systems while maintaining design flexibility and overcoming some of the limitations of monolithic integration.

The choice between monolithic and heterogeneous integration depends

on various factors, including performance requirements, cost considerations, and the specific application domain. Both approaches hold promise for the future development of compact, high-performance OPA-LiDAR systems, and continued research in this area will likely lead to further advancements in the integration of electronics and photonics on a single chip.

1.7 Building an OPA

1.7.1 Grating Coupler

Gratings are periodic structures created on a surface by altering either the material composition or the surface topography. In silicon-on-insulator (SOI) photonic chips, gratings are formed by selectively etching or depositing amorphous silicon onto the SOI layer.This process induces variations in the refractive index, enabling light manipulation. When the period of these index variations exceeds the wavelength of light within the grating, diffraction becomes the dominant effect. Conversely, if the period is smaller, light propagation resembles that in a uniform medium, an effect that intensifies as the period shrinks. Grating couplers, as illustrated in Figure 1.6 operate within the diffraction regime[25].

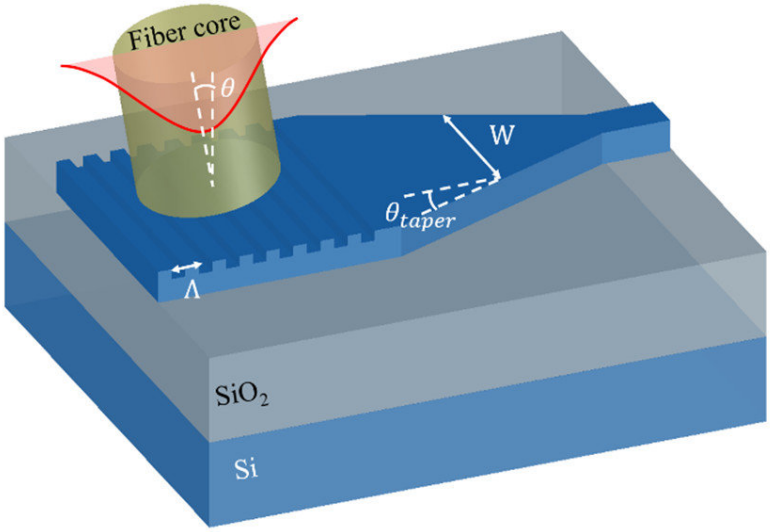

Figure 1.6: Schematic structure for a 1D grating coupler (GC) with linear waveguide taper and key parameters: period Λ, fiber tilt angle θ, varying taper width W and taper angle θtaper [26].

For a surface grating coupler (GC) with refractive index variations along a single direction, termed a 1D-GC, light couples into the direction of this variation. To simplify the analysis of diffraction GC principles, we focus on 1D-GCs, recognizing that the underlying theory also applies to 2D-GCs when at least one propagation direction is in the diffraction regime. However, if both directions of a 2D-GC operate in the diffraction regime, light can propagate bi-directionally, and the principles of 1D-GCs apply to each direction independently.

Bragg Condition

As illustrated in Fig. 1.7(a),the diffraction behavior of a grating coupler (GC) can be comprehensively understood through the Bragg condition, also known as the phase-matching condition. This condition illuminates the relationship between the wave-vector (k_0) of an incident light beam above the chip and the propagation constant (β) of the coupled light beam within the waveguide, which is essential for efficient light coupling. Mathematically, the Bragg condition is represented as:

$$\beta = k_0 + mG \tag{1.6}$$

where G symbolizes the grating vector and m signifies the grating diffraction order. A wave-vector diagram, as depicted in Figure 1.7(b) for fiber-to-chip coupling, visually elucidates this relationship. A similar analysis can be applied to the chip-to-fiber coupling scenario. While the Bragg condition effectively predicts the allowed diffraction order, it does not provide insight into the energy distribution between orders or the diffraction efficiency. Typically, coupling efficiency (CE) is determined using numerical methods like finite-difference time-domain (FDTD) calculations. However, a qualitative estimate of CE can be obtained by analyzing the major power loss channels, as illustrated in Figure 1.7(a). For input coupling, as depicted on the left side of Figure 1.7(a), a portion of the uncoupled power (Psub) is lost to the substrate, despite potential reflections due to constructive interference at the oxide layer. Additional power losses occur due to reflection (Pr) in the opposite direction of the incident beam, and coupling (Pw2) in the opposite direction of the waveguide, particularly for perfectly vertical incidence. Consequently, the final power coupled into the waveguide (Pw) can be expressed as:

$$Pw = \eta\text{CEPin} = \text{Pin - Psub - Pr - Pw2} \tag{1.7}$$

where ηCE represents the coupling efficiency, often expressed as coupling loss in decibels (dB).A similar analysis can be applied to chip-to-fiber

out-coupling, as shown on the right side of Figure 1.7(a)[27]. Here, CE is usually described in terms of directionality (Pup/Pw), representing the fraction of waveguide power diffracted towards the fiber, and modal overlap, referring to the portion of upward-directed power successfully launched into the fiber.

$$Pout = \eta \text{CEPw} = (\eta)(\text{Pw - Pt - Pr}) \tag{1.8}$$

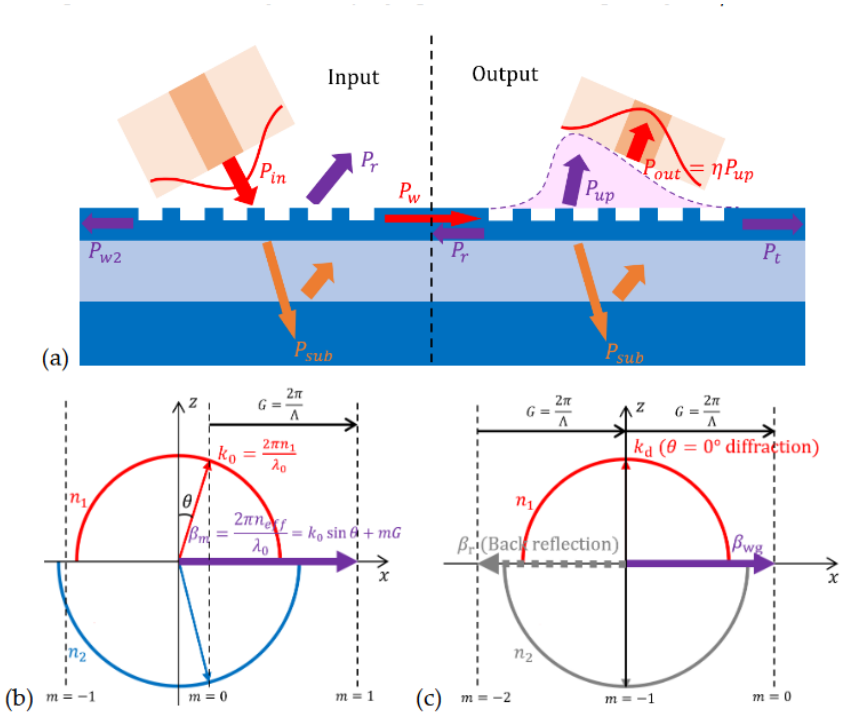

Figure 1.7: (a) Loss channels in input and output coupling; (b) wave-vector diagram for fiber-to-chip coupling; and (c) wave-vector diagram for chip-to-fiber perfectly vertical coupling [28].

Although the Bragg condition allows for perfectly vertical coupling (θ=0), a fiber tilt angle is often employed. In the chip-to-fiber case, this is due to strong backward reflection caused by second-order diffraction, as illustrated by βr in the wave-vector diagram (Figure 1.7(c))[29][30]. This reflection significantly diminishes CE for a perfectly vertical GC. Conversely, in the fiber-to-chip case, grating symmetry leads to bi-directional propagation of coupled light for diffraction orders m = 1 and m = -1. However, fiber attachment without tilt is preferred in packaging, prompting many studies to focus on enhancing the performance of perfectly vertical GCs. Efficient coupling

is a critical factor in silicon photonics, with grating couplers (GCs) and edge couplers being the two prevalent coupling schemes.

While GCs offer advantages in terms of flexibility, ease of fabrication and testing, they fall short in coupling loss, polarization sensitivity, and wavelength diversity compared to edge couplers.Despite these drawbacks, GCs find widespread use in various applications beyond simple fiber-to-chip coupling. They are instrumental in enabling coupling between different integrated layers on a chip, as well as between on-chip light sources and waveguides.Furthermore, GCs have been successfully implemented in diverse fields, including biomedical sensing and LiDAR, demonstrating their versatility and potential for broader impact.

1.7.2 Phase Shifters

The increasing complexity of photonic integrated circuits (PICs) demands efficient and high-performance on-chip active components to enable sophisticated functionalities. Among these components, phase shifters stand out as crucial building blocks in large-scale PICs. These phase shifters are designed to exclusively modulate the phase of a transmitted wave without altering its amplitude, while power tuning can be achieved by incorporating them into interferometers. A sufficient number of such building blocks can be utilized to construct arbitrary linear optical systems, leading to a wide range of applications.Researchers have successfully demonstrated various applications using well-integrated phase shifters, including neuromorphic computing systems, optical phased arrays, LiDAR systems, on-chip spectrometers, and photonic accelerators.

Phase Shift principle

The phase shift of the optical wave in the waveguide can be obtained by

$$\Delta_\phi = \frac{\Delta\text{neff}\ 2\pi\ \Delta\ \text{L}}{\lambda} \tag{1.9}$$

Thermo-optic phase shifters are a key component in silicon photonics, altering the effective refractive index (Δneff) of the optical mode through temperature-induced changes in the material's refractive index. This is achieved by integrating on-chip heaters, which allow for precise control over the temperature and, consequently, the optical phase. Electro-optic phase shifters leverage the electro-optic effect, where the application of an electric field directly alters the material's refractive index, leading to a change in the effective refractive index (Δneff) of the optical mode. This precise electrical control over the

refractive index enables rapid and accurate phase modulation in integrated photonic devices.

Working Principle of Thermo-Optic Phase shifters

Thermo-optic phase shifters operate on the principle of modifying the refractive index of both the waveguide and cladding materials by passing a current through an integrated resistive heater. This induced temperature change subsequently alters the effective refractive index of the propagating optical mode, resulting in a controllable phase shift[31]. The relationship between the phase change and the temperature change can be mathematically expressed as...

$$\Delta_{\phi}(\Delta T) = (\frac{2\pi}{\lambda})(\frac{\mathrm{dn}}{\mathrm{dT}}) \tag{1.10}$$

where λ is the wavelength, and (dn/dT) neff is the change in the effective refractive index of the transmission mode versus the change in temperature. This coefficient is not only affected by the change in the refractive index of silicon, but also the change in the refractive index of the surrounding claddings (e.g., silicon dioxide, silicon nitride). Δ T is the change in the temperature and L is the length of the heating waveguide region. According to Equation (1.10), the required temperature change to achieve p phase shift is:

$$\Delta T_{\pi} = (\frac{2\lambda}{2\mathrm{L}})(\frac{\mathrm{dT}}{\mathrm{dn}}) \tag{1.11}$$

Thus, one of the FOMs, the power consumption, can be approximately given by

$$\Delta P_{\pi} = \Delta T_{\pi}.G \tag{1.12}$$

where G is the thermal conductance between the heated waveguide and the heat sink in a unit of W/K.Two other important figures of merit are the propagation loss of the waveguide and the modulation speed. The modulation speed can be evaluated by a time constant, which is determined by

$$\tau = \frac{\mathrm{H}}{\mathrm{G}} \tag{1.13}$$

where H is the heat capacity of the heated arm. The gap of finite thermal conductance between the heat source and the waveguide is not considered in the above equations. A typical configuration for a thermo-optic phase shifter is depicted in Figure 1.8(a)[32][33]. Here, the silicon waveguide is embedded within a cladding layer, and a heater is positioned above the waveguide.To mitigate optical insertion loss, the vertical spacing between the heater and

waveguide must be sufficiently large. Therefore, an upper cladding layer is commonly deposited, both to isolate the metal heater and provide structural support for the waveguide. When designing thermo-optic phase shifters, careful consideration must be given to the width of the silicon waveguide, as well as the thickness and material composition of both the cladding and heater layers. Building upon the traditional thermo-optic phase shifter design, numerous research efforts have focused on optimizing key performance metrics, namely power consumption, modulation speed, and insertion loss, as illustrated in Figure 1.8[34]. Figure 1.8(b) showcases a strategy for enhancing power consumption by thermally isolating the silicon waveguide from the surrounding claddings and substrate through the implementation of a free-standing waveguide. In contrast, Figure 1.8(c) demonstrates an approach to improve both power consumption and modulation speed by minimizing the vertical gap between the heater and the bus waveguide. This design necessitates the use of optically transparent materials, such as 2D materials, to prevent significant propagation loss. Figure 1.8(d)(e) highlights the use of doped silicon as an alternative heater material, offering a promising balance between these three critical figures of merit (FOM).

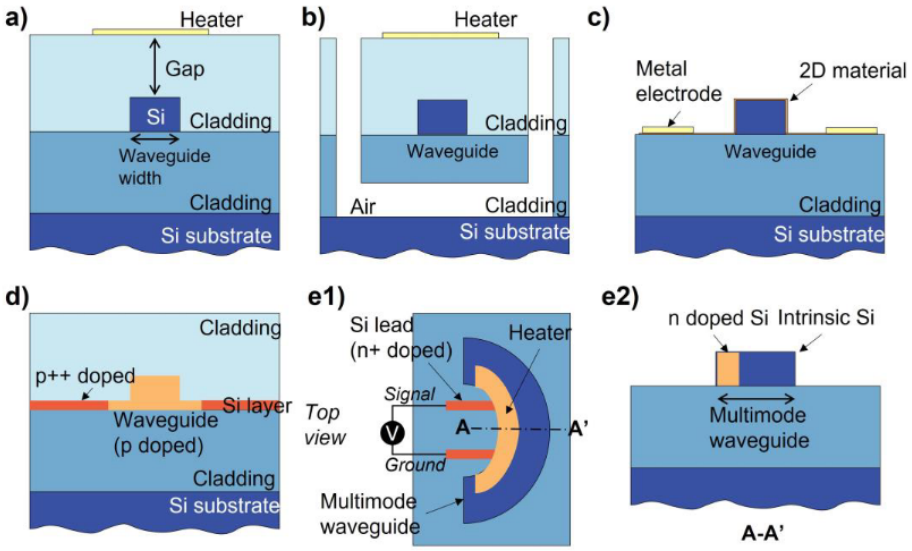

Figure 1.8: Various structures of thermo-optics phase shifters. (a) Traditional thermo-optics phase shifter, (b) thermo-optics phase shifter with air trench, (c) thermo-optics phase shifter with 2D material heaters, (d) thermo-optics phase shifter with doping silicon heater, (e1) bended thermo-optics phase shifter with doping silicon heater and (e2) its cross-sectional schematic [35].

Beyond structural considerations, the choice of heater material is crucial for thermo-optic phase shifter performance. Commonly used heater materials include metals, which are placed atop the bus waveguide, and doped-silicon resistors, positioned on either side of the waveguide. Experimental results from thermo-optic phase shifters fabricated in the IMEC and AMF commercial foundries reveal comparable modulation efficiencies for both metal and doped-silicon heaters. However, doped-silicon heaters exhibit faster modulation speeds, albeit with a larger footprint. In addition to traditional materials, optically transparent materials like graphene and ITO are also attractive candidates for heaters, due to their exceptional optical properties and high electrical resistance.

Working Principle of Electro-Optic Phase shifters

An electro-optic phase shifter is an active photonic device that manipulates the phase of light by utilizing the electro-optic effect. In this effect, an applied electric field induces a change in the refractive index of the material through which the light propagates. By modulating the applied electric field, the phase of the transmitted light can be precisely controlled, enabling a range of functionalities such as signal routing, switching, and interferometry in integrated photonic circuits. Electro-optic phase shifters primarily utilize the plasma dispersion effect. Silicon optical modulators, as depicted in Figure 1.9, can be categorized into three distinct types based on the electrical manipulation of free carriers interacting with light within the silicon waveguide: carrier accumulation1.9(a), carrier injection 1.9(b), and carrier depletion1.9(c)[36]. The carrier-accumulation and carrier-depletion types employ semiconductor-insulator-semiconductor (SIS) and pn junction structures, respectively, making them more suitable for high-speed modulation due to their majority-carrier-based operation, in contrast to the carrier-injection type, which relies on a pin junction. While the carrier-accumulation modulator necessitates an oxide barrier, the carrier-depletion type only requires a readily CMOS-compatible pn junction. Consequently, the carrier-depletion approach has gained prominence due to its relative ease of fabrication and simplified design[4][37].

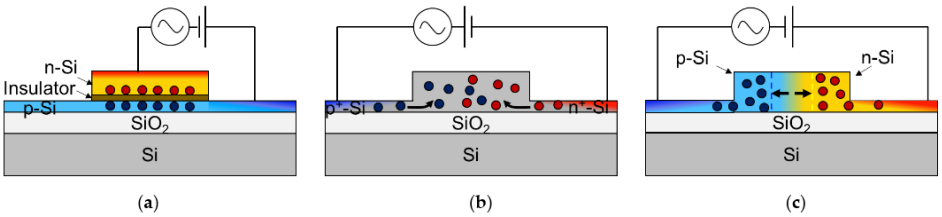

Figure 1.9: Cross-sections of typical device structures implementing the three different mechanisms (a) Carrier accumulation, (b) Carrier injection, and (c) Carrier depletion [38].

The limitations of silicon modulators, as highlighted above, underscore the importance of exploring heterogeneous integration, leveraging materials with superior electro-optic properties alongside the established silicon photonics platform. One such promising material is silicon germanium (SiGe). Due to the inverse relationship between the change in refractive index and the effective masses of electrons and holes in the plasma dispersion effect, lighter conductivity masses lead to greater plasma dispersion. In CMOS technology, the application of strain to silicon is a well-established technique to achieve lighter conductivity masses and higher mobilities in transistor channels, thereby enhancing performance. Tensile and compressive strains are introduced to silicon for n-channel and p-channel MOS transistors, respectively. Notably, prior research has demonstrated that uniaxial strain applied to silicon can modify both the plasma dispersion effect and free-carrier absorption in the far-infrared wavelength range, highlighting the potential of strain engineering for modulating optical properties.

In this context, strained SiGe has gained recognition as a p-channel material in CMOS technology due to its high hole mobility, stemming from the low effective mass of holes. Consequently, SiGe is expected to exhibit an enhanced plasma dispersion effect, offering promising avenues for improved electro-optic modulation in integrated photonic devices.

1.7.3 Splitters

Y-BranchSplitters

The Y-branch waveguide, a fundamental integrated optical component, comprises one input and two output waveguides, enabling the confinement, distribution, and propagation of photons within the waveguide structure. A symmetrical longitudinal design allows for uniform power splitting, while optimization of the basic Y-branch structure, such as employing a multimode

tapered branch instead of a standard Y-branch, can further enhance performance. By segmenting the branch geometry into multiple optimizable width values, the tapered branch model demonstrates a notable 4 dB improvement over the conventional model. This enhancement applies across a 1260 nm to 1360 nm wavelength range, with significant gains in both output port bandwidth and power uniformity. Moreover, asymmetric branch designs enable the achievement of arbitrary power output proportions. Furthermore, integrating specific structures with the standard Y-branch waveguide can unlock additional functionalities, including polarization beam splitting. These versatile properties make the Y-branch waveguide a valuable building block in a wide array of optical applications.

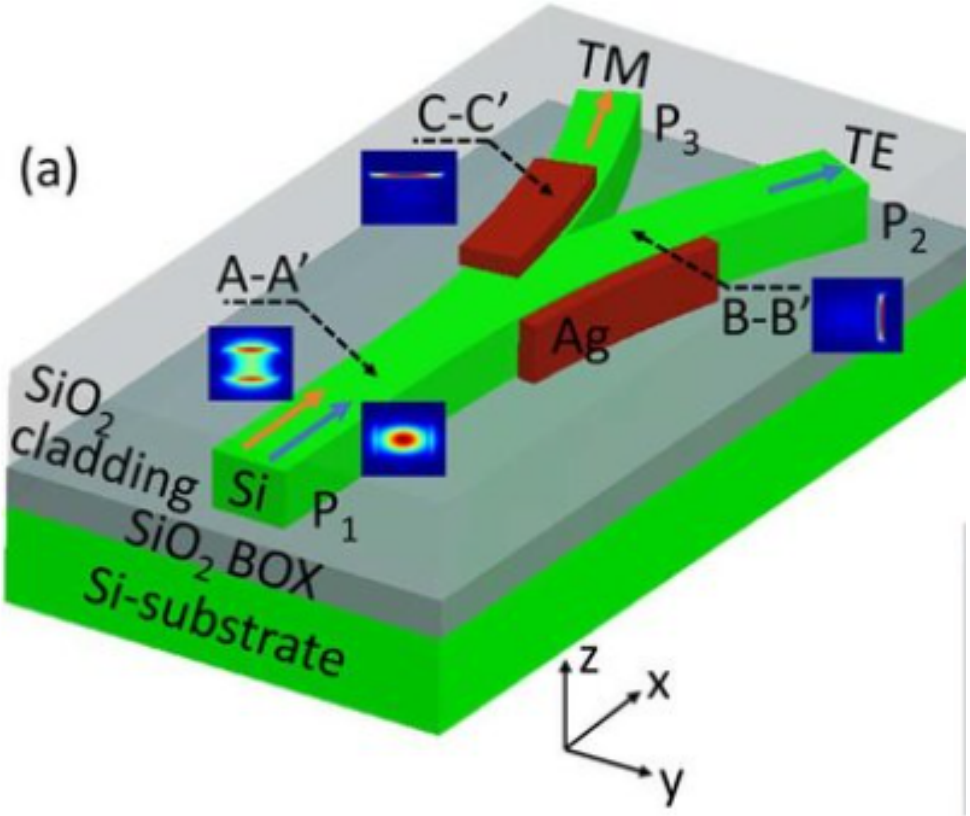

Figure 1.10: Optimal design of y-branch beam splitter, Structural diagram of y-branch polarization beam splitter of hybrid plasma waveguide [39] .

Hu's 2016 hybrid plasmonic Y-branch (HPYB) waveguide design (Figure 1.10) offers a wavelength-insensitive polarization splitter. By incorporating

Ag strip waveguides on the traditional Y-branch's side and upper surface, the HPYB enables excitation of vertical and horizontal hybrid plasmon modes for input TE and TM modes, respectively. This compact device boasts a wide 285 nm bandwidth and a substantial 210 nm fabrication tolerance.

An alternative approach to polarization beam splitting, proposed in 2017, leverages a polymer waveguide and a high-birefringence material. The relative refractive indices of these materials vary with the mode, facilitating the separation of TE and TM polarizations. In the device illustrated in Figure 1.11, the "Reactive Mesogen (RM)" birefringent material is embedded within a Y-branch optical waveguide, selectively extracting the TE polarized mode. The RM's higher refractive index for TE polarization, compared to the CO-polymer waveguide, guides TM polarized light along the CO-polymer waveguide while coupling TE polarized light into the RM waveguide via a taper structure.

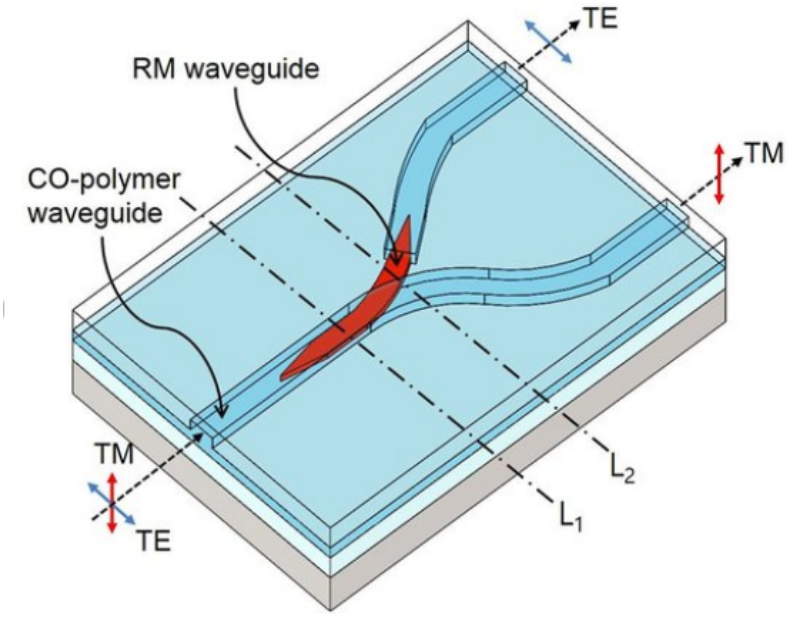

Figure 1.11: Schematic diagram of polarization beam splitter inserted with high birefringence material [40].

1.8 Organization of the Thesis

This section provides an overview of how the thesis is organized. The thesis consists of four chapters whose contents are as follows:

Chapter 1 This chapter provides an introduction to the various topics

which are necessary in understanding the need for the thesis work. The chapter also describes the motivation and objective of the thesis work.

Chapter 2 This chapter reviews prior work on optical phased arrays (OPAs) for beam steering.Research has explored various materials, phase shifting mechanisms, and antenna configurations, demonstrating both 1D and 2D beam steering with varying performance metrics.

Chapter 3 This chapter presents the design and simulation of a compact 16-channel optical phased array (OPA) utilizing Si-ITO phase shifters for enhanced beam steering. FDTD simulations demonstrate a lateral steering range of 56° and longitudinal steering of 23° through wavelength tuning. The device, with a footprint of 0.07 mm x 0.02 mm, highlights the potential of Si-ITO in realizing compact, high-performance OPAs for LiDAR applications.

Chapter 4 This chapter outlines the thesis and briefly discusses the future scope of the project.

Chapter 2

Literature Survey

2.1 Introduction

Optical beam shaping and steering technologies are crucial for diverse applications. Free-space optical communication relies on these technologies to transmit secure, high-speed data over long distances. LiDAR systems, used in remote sensing and emerging technologies like autonomous vehicles, leverage beam steering for 3D imaging and mapping. Additional applications include imaging systems, electronic warfare, lithography, and additive manufacturing. Traditional beam steering systems based on opto-mechanical assemblies are often bulky, expensive, and slow. While advancements like MEMS and liquid-crystal spatial light modulators offer some miniaturization, their speed remains a limiting factor.

Photonic integrated circuits (PICs), utilizing optical phased array (OPA) technology, present a promising path towards compact, high-speed, and potentially high-power beam steering systems. This review explores the current state-of-the-art in PIC-based beam steering, focusing on key metrics like beam width, steering angle, and power scaling.Traditional systems that generate, shape, and steer narrow optical beams are often large and complex due to their reliance on mechanical parts. These systems are also costly, relatively slow, and easily affected by environmental changes. While smaller systems using micro-mirrors (MEMS) or liquid crystals exist, they are still limited in speed. Researchers are developing photonic integrated circuits (PICs) using optical phased array (OPA) technology to create compact, fast, and potentially powerful beam steering systems.

2.2 Beam Steering using Tuning in Wavelength and Phase shift

Beam steering through wavelength tuning is a dynamic process reliant on various critical parameters within the system. The effective refractive index of the waveguide, the grating pitch, the refractive index of the cladding, and the input wavelength collectively influence this mechanism. By adjusting the wavelength, precise control over beam steering is achieved. The effective refractive index of the waveguide plays a pivotal role in determining the path of the light, while the grating pitch influences diffraction and dispersion effects. Additionally, the refractive index of the cladding contributes to the confinement and propagation of the light within the waveguide structure. By carefully manipulating these factors and employing wavelength tuning, a high level of control and accuracy in beam steering is attained,Lateral steering in phased array systems is achieved by systematically introducing a progressive phase difference across the array elements, facilitated by electro-optic or thermo-optic phase shifters. This cumulative phase shift induces a corresponding lateral displacement of the resulting beam. The magnitude and direction of this beam deflection are directly proportional to the applied phase difference, enabling precise and dynamic control over the beam's trajectory.

2.3 Review of OPA

Weihua Guo, et.al-2013 [41]

This work demonstrates a novel approach to two-dimensional optical beam steering using an indium phosphide (InP) photonic integrated circuit (PIC). The PIC leverages a 1-D phased array of eight semiconductor optical amplifiers (SOAs) for lateral steering, achieving deflection angles up to ±10° by precisely controlling the phase shift in each channel.Longitudinal steering is accomplished by adjusting the emission angle of surface gratings through tuning the wavelength of either an external or an integrated sampled-grating distributed Bragg reflector (SGDBR) laser, exhibiting an efficiency of 0.14°/nm. The PIC architecture includes on-chip photodiodes to monitor interference between adjacent channels, facilitating accurate phase calibration and control for the SOA array. The system showcases high-speed beam steering exceeding 10^{7}°/s, made possible by the fast response of both SOAs and the tunable laser. The integration of an SGDBR laser onto the chip streamlines the system and enables broader wavelength tuning potential for future development. This research addresses challenges like grating reflections and side-lobe suppres-

sion while suggesting solutions such as non-uniform grating spacing and lens magnification to achieve larger steering angles and improved beam quality, paving the way for practical implementations in LIDAR and other applications.

Kwong, et.al-2014 [42]

This work presents a significant advancement in chip-scale optical beam steering technology.The researchers demonstrate a 16-element optical phased array (OPA) integrated onto a silicon-on-insulator (SOI) platform, capable of two-dimensional (2D) beam steering.The device leverages the SOI platform's mature semiconductor fabrication processes, enabling the integration of complex photonic circuitry while maintaining a compact footprint (1 mm x 9 mm). Beam steering is achieved through a combination of two mechanisms. By varying the input wavelength from 1480 nm to 1580 nm, the emission angle of the waveguide gratings is adjusted, achieving longitudinal (θ) steering up to 15°.Each waveguide is equipped with an independent metal micro-heater. By applying varying voltages, the refractive index of the silicon waveguide is modified through the thermo-optic effect. This introduces phase differences between array elements, resulting in lateral (ϕ) steering up to 20°. A key innovation lies in the output grating couplers. Traditionally, shallow-etched gratings have been used to achieve efficient coupling to free space. However, these require precise etching control. The researchers instead employed a polycrystalline silicon (polysilicon) overlay with an oxide etch-stop layer. This simplifies fabrication significantly while still achieving narrow far-field beam widths (1.2° x 0.5°) crucial for precise beam steering.The OPA demonstrates 2D steering across a 20° x 15° field of view with a sidelobe level better than -10 dB. Each thermo-optic phase shifter requires a switching power of 20 mW for a π phase shift. The rise time of the phase shifters is measured to be 48 μs, corresponding to a modulation bandwidth of 7.3 kHz.

The research addresses the challenges of phase errors due to fabrication imperfections by implementing a closed-loop feedback control system using a LabVIEW interface and an IR camera. This allows for real-time optimization of the applied voltages to each phase shifter, maximizing the power directed towards the desired steering angle.

J. C. Hulme, et.al-2015 [43]

The research presents the first fully-integrated 2D beam-steering chip on a hybrid silicon platform.Integrating over 164 components, including lasers, amplifiers, phase shifters, and grating couplers, the chip demonstrates beam

steering over a 23° x 3.6° range. Lateral steering is achieved using a 32-channel optical phased array (OPA) with p-i-n silicon diode phase shifters, primarily operating in the thermo-optic regime. Longitudinal steering is accomplished by tuning the on-chip laser's wavelength over 34.5 nm, resulting in steering of 3.6° via surface gratings.Two grating coupler configurations were investigated: a uniform array with a 4 μm pitch and a Gaussian array with a varying pitch. The total aperture size, estimated from the emitter array width, is approximately 128 μm for the uniform array and 168 μm for the Gaussian array. Although the on-chip photodiode array for feedback faced fabrication challenges, the chip successfully achieved a 1° x 0.6° beam width and greater than 70% background suppression, resulting in 138 resolvable spots.This work represents a significant step towards miniaturized, solid-state beam steering systems. Potential applications include LIDAR, free-space communications, and biomedical imaging, where the chip's compact size, high resolution, and integrated design could revolutionize current technologies.

V. Poulton, et.al-2016 [44]

This research presents a significant advancement in the field of optical phased arrays (OPAs) by demonstrating a record-breaking 50-element device. This achievement is facilitated by a novel architecture employing grouped cascaded phase shifters, enabling precise beam steering with simplified control mechanisms. Each grating coupler, spaced 2 μm apart, is paired with a thermal phase shifter, contributing to a compact overall footprint of 1200 μm x 200 μm. A key innovation lies in the division of cascaded phase shifters into three distinct groups. This approach not only compensates for fabrication-induced phase noise but also allows for finer control over beam steering. By manipulating individual group voltages, researchers achieved a record-breaking two-dimensional steering range of 46° (lateral) and 36° (longitudinal) while maintaining a remarkably small spot size of 0.85° x 0.18°.The OPA utilizes full-etch silicon gratings to ensure uniform emission across a broad wavelength range of 1454 nm to 1641 nm. Despite the presence of strong grating lobes due to antenna design imperfections, the array achieves a commendable 1mW beam power. This power level, combined with the OPA's steering capabilities, enables the demonstration of a lens-free free-space data link operating at 1 Mbps.The implications of this research are far-reaching. The demonstrated performance metrics position this OPA as a prime candidate for applications in LIDAR, free-space optical communications, and high-resolution imaging. Future refinements to the antenna design, aimed at mitigating grating lobes, promise to further enhance the OPA's capabilities and

solidify its position as a technological breakthrough in the field of integrated photonics.

DAVID N , et.al-2016 [45]

This research presents a groundbreaking advancement in optical phased array (OPA) technology,demonstrating a two-axis steerable device with unprecedented steering range and resolution. Traditional OPAs face a tradeoff between wide steering angles and narrow beam divergence (high resolution). This work overcomes this limitation by employing non-uniform emitter spacing, a strategy borrowed from radar phased arrays.The OPA consists of 128 emitters fabricated in a 300 mm CMOS process. Each emitter is equipped with a thermo-optic phase shifter, enabling precise control of the emitted light's phase. By arranging the emitters in a non-uniform pattern, the researchers suppress unwanted grating lobes, which typically restrict the steering range. This allows for an impressive 80-degree steering in the phased-array axis, limited only by the measurement setup's numerical aperture.The device achieves exceptional resolution (over 500 resolvable spots) in the phased-array axis due to the large number of phase-controlled emitters and the resulting narrow beam divergence of 0.14 degrees. Additionally, by utilizing a shallow grating etch for the emitters, the OPA achieves a record-low beam divergence of 0.142 degrees in the wavelength-steered axis. Combining phase and wavelength steering, the device can address over 60,000 resolvable points in two dimensions.The research demonstrates the OPA's steering capability across a 100 nm wavelength range (1260 nm to 1360 nm), achieving a 17-degree steering angle in the wavelength-controlled axis. This broad wavelength tuning range is particularly promising for integration with on-chip tunable lasers, further enhancing the OPA's versatility.

Y INGZHI LI , et.al-2021 [46]

This research introduces two novel 128-channel optical phased arrays (OPAs) designed for solid-state beam steering in LiDAR applications. The OPAs, fabricated on a silicon nitride-on-silicon (SiN-on-SOI) platform, utilize either a fishbone or chain antenna structure. These dual-level waveguide grating antennas are designed to achieve a wide field of view (FOV), high resolution, and efficient light emission.A key innovation is the use of nonuniform antenna pitch, allowing for a large 4 mm aperture with only 128 waveguides, reducing system complexity and power consumption. This design also enables wide lateral steering ranges: ±70° for the chain antenna OPA and ±50° for the fishbone antenna OPA.The OPAs achieve wavelength steering in the

ϕ direction by tuning a laser over a 1350-1630 nm range, resulting in a steering range of approximately 19°. Notably, the fishbone antenna OPA boasts a very small longitudinal divergence of 0.029°, a significant advancement in OPA technology.The phase shifters employed are p-n junctions operating at reverse voltage, offering low power consumption (maximum 1.8 μW) and high-speed modulation.To demonstrate the OPAs' potential in real-world applications, they were integrated into a frequency-modulated continuous-wave (FMCW) LiDAR system. This system successfully measured distances up to 100 meters, highlighting the OPAs' capability for long-range detection with low nonlinearity thanks to the Si3N4 waveguide. The results confirm that these OPAs are promising candidates for transceiving optical signals in LiDAR systems, with potential to revolutionize solid-state beam steering in various fields.

2.4 Research Objectives

Despite significant progress in beam steering using optical phased arrays (OPAs), a comprehensive review of existing literature reveals that substantial improvements are still required to achieve a combination of wider steering angles, smaller divergence angles, and compact aperture sizes and following are the some research objectives and carried out for the Thesis

- Grating coupler optimization: The study demonstrates the impact of grating pitch and duty cycle on the far-field radiation patterns of single grating couplers, identifying optimal parameters for achieving focused beams with minimal side lobes.
- Scalable OPA design: A scalable design approach for multi-channel OPAs (2, 4, 8, and 16 channels) by cascading splitters, achieving relatively equal power splitting ratios among channels and improving beam directivity with increasing channel count.
- Wavelength tuning for longitudinal steering: Longitudinal beam steering was achieved through wavelength tuning in longitudinal direction, demonstrating the OPA's adaptability for dynamic beam control.This wavelength-dependent steering capability arises from the varying diffraction angles experienced by different wavelengths at the grating couplers, making it suitable for applications requiring precise beam direction control, such as LiDAR systems.

- Si-ITO phase shifters for lateral steering: The utilization of Si-ITO phase shifters enables precise lateral beam steering , highlights the potential of this material for compact, high-performance OPA designs.

Chapter 3

Chip scale Optical Beam Steering

3.1 Introduction

Optical phased arrays (OPAs) facilitate beam steering through precise manipulation of light. Key components include a coherent light source, a beam splitter to distribute the light, phase shifters (either thermal or electro-optical) to modulate individual beams, and grating couplers to emit the combined beam. Two-dimensional steering is achieved by adjusting both wavelength and phase: tuning the source wavelength alters the longitudinal angle, while varying phase delays across grating couplers controls the lateral direction.

3.2 Proposed OPA

The proposed device as shown in Figure 3.1is tailored to support the fundamental TE-mode throughout the near-infrared wavelength range. Light enters through input waveguide and then separates into numerous channels employing Multi-Mode Interference devices (MMIs). Positioned at the termination of the MMIs is the Electro-Optic phase shifter. This phase shifter consists of n-type ITO on p-type Silicon. The characteristics of ITO material are as follows: DC permittivity of 3.9, a work function of 5.4 eV, a bandgap measuring 3.8 eV, electron mobility of 41 cm^2/V s, hole mobility of 9.5 cm^2/V s, refractive index of 1.3 with an imaginary component of 0.036, and an effective mass of 0.35. the length, width and thickness of ITO are L_{ITO} is 10 μm, W_{ITO} is 0.6 μm t_{ITO} is 0.15 μm [47][48][49]. The characteristics of p-type Silicon are as follows DC permittivity 11.9; Work function 4.6 eV; Bandgap 1.1 eV; electron-mobility 62.5 cm^2/Vs; refractive index 3.4207. The length, width and thickness of p-type silicon is L_{Si} is 10 μm W_{Si} is 0.6 μm t_{Si} is 0.15 μm. The device having grating period (Λ) of 0.73 μm, maintaining an equal

duty ratio. The silicon grating width ($W_{Grating}$) of 0.6 μm, and the total length of the grating extends to L Grating 30 μm. The top of grating is array is SiO2 having width and length 0.6 μm and 30 μm. The thickness of SiO2 is 0.5 μm. The pitch d is set to 0.775 μm which is equal to $\lambda/2$ for a wide steering along longitudinal axis (θ). The Si-ITO electro-optic phase shifters in Proposed device operates by harnessing the unique properties of silicon (Si) integrated with indium tin oxide (ITO) to manipulate the phase of light in response to an electric field. This innovative device capitalizes on the electro-optic effect present in ITO, which, when combined with silicon's compatibility and structural advantages, offers a compelling solution for optical modulation. Upon application of an electric field, ITO exhibits change in its refractive index, inducing a corresponding alteration in the phase of light passing through it. This collaborative synergy between silicon and ITO allows for precise and rapid adjustments in the optical phase, providing a platform for agile signal processing and manipulation within optical systems. The Si-ITO electro-optic phase shifter stands as a testament to advancements in material engineering, paving the way for compact, efficient, and adaptable devices crucial for the evolution of optical communication networks and photonic applications.The use of Si-ITO in electro-optic phase shifting replacing the conventional Si phase shifters, directly tackles inherent limitations . Traditional Si-based phase shifters face challenges with poor electro-optic effects, larger device footprints, demanding driving voltages, and subpar performance, sparking intensive research to overcome these barriers. Achieving compact modulators holds paramount importance in advancing on-chip packaging density. dimensions of ITO used for phase shifter is chip scale and helped to refine the beam steering capabilities. This Si-ITO phase shifter component contributed to the controlled manipulation of the emitted light, facilitating precise lateral beam steering (ϕ) and the beam's lateral direction could be dynamically adjusted, adding an extra layer of adaptability and control to the overall design.

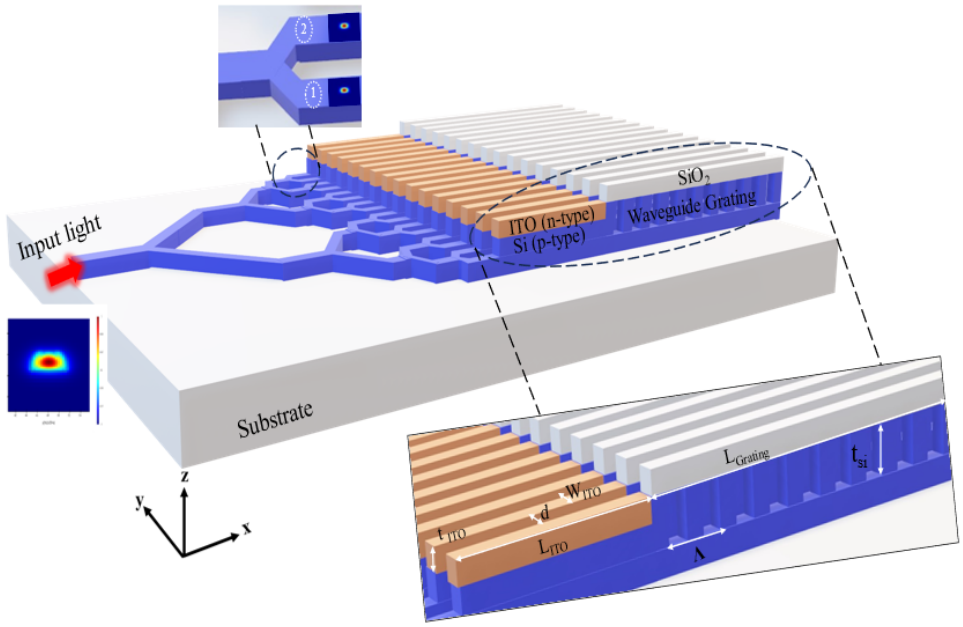

Figure 3.1: 3D schematic representation of the proposed 16-channel optical phased array featuring the initial light source and showcasing its mode profile. Top insect shows 1X2 Y-Splitter displaying the mode profiles on its two output ports. Bottom insect depicts the enlarged view of the selected section from the 3D schematic representation.

3.3 Design of Grating Coupler

The angle θ shown in Figure 3.2 at which light diffracts from a grating coupler is determined by several design parameters, including the grating pitch (Λ), effective index of the grating (neff), incident laser wavelength (λ), and the refractive index of the cladding (nclad), as described by the equation

$$sin\theta_{max} = \frac{\Lambda\text{neff-}\lambda_0}{\text{nclad}} \tag{3.1}$$

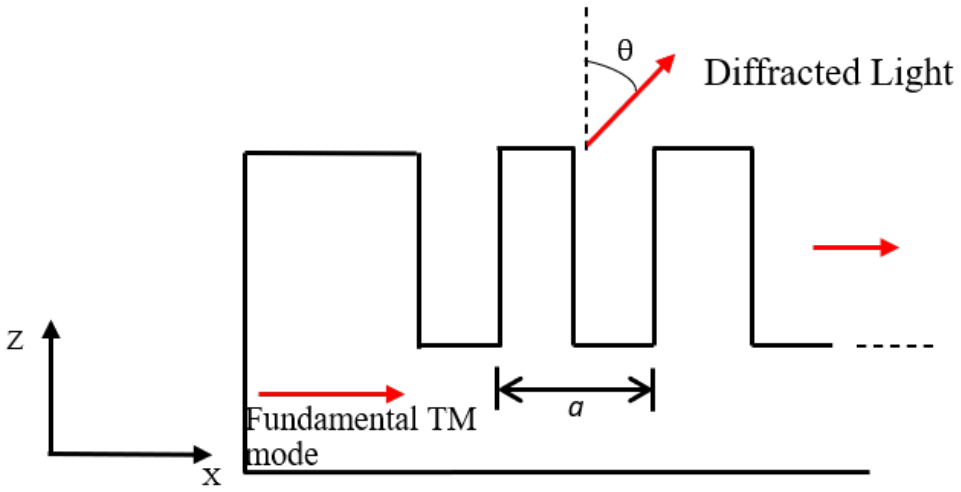

Figure 3.2: Side View of Grating Coupler

3.3.1 Effect of Grating Period

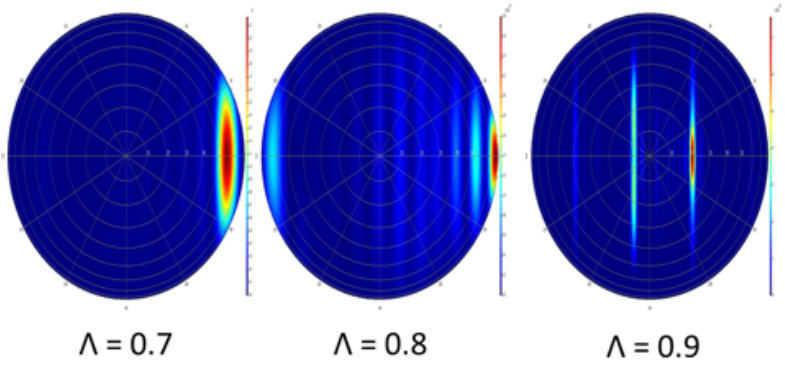

Figure 3.3: FDTD simulations showing the effect of grating pitch (Λ) on diffraction angle in an optical phased array.Increasing pitch from 0.7 to 0.9 reduces the diffraction angle, concentrating the beam towards the center.

Figure 3.3 impact of grating pitch (Λ) for a grating coupler designed for a 1.55 μm light source. Three distinct grating pitches, corresponding to 0.7, 0.8, and 0.9, were evaluated. Results reveal a clear decrease in diffraction angle with increasing pitch, consistent with theoretical expectations. Notably, at $\Lambda = 0.7$, the diffraction pattern closely resembles that of a single emitter, suggesting efficient power coupling. However, when Λ exceeds $\lambda_0/2$ (as seen in the Λ

= 0.9 case), grating lobes emerge, significantly impacting the beam's directionality and intensity. These findings underscore the critical role of grating pitch selection in achieving optimal beam steering performance and minimizing unwanted artifacts in OPA-based LiDAR systems.

3.3.2 Effect of Duty Cycle

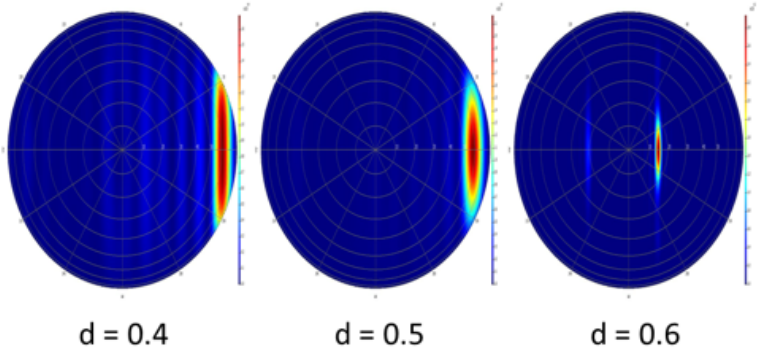

Figure 3.4: FDTD Simulation Results of a Single Grating Coupler: Investigating the Impact of Duty Cycle (d) on Far-Field Radiation Patterns. The duty cycle is varied across three values (0.4, 0.5, and 0.6) while maintaining a constant wavelength (λ_0 = 1.55 μm) and cladding refractive index (nclad). Results reveal a narrowing of the main lobe and an increase in side lobe intensity as the duty cycle increases.

The figure 3.4 illustrates the impact of duty cycle on the far-field radiation patterns of a single grating coupler, obtained through FDTD simulations. Three duty cycles (0.4, 0.5, and 0.6) were examined while keeping the wavelength (λ_0 = 1.55 μm) and cladding refractive index constant. Results reveal a clear trend: as the duty cycle increases, the main lobe of the radiation pattern becomes narrower, indicating increased beam focus. However, this is accompanied by a rise in side lobe intensity. These findings highlight that a duty cycle near 0.5 strikes an optimal balance between beam focus and minimal side lobe effects, crucial for applications like LiDAR that demand precise beam steering.

Figure 3.5 (a) illustrates the YZ view of the grating coupler as simulated in Mode Solutions. for λ = 1550 nm,cladding refractive index =1.44 ,neff of GC=2.91, d=0.5 (Calculated from Ansys Model Solutions) Grating Pitch (Λ) =0.73 μm the diffracted angle θ should be equal to 39° from which is exactly same as shown in Figure 3.5 (b)

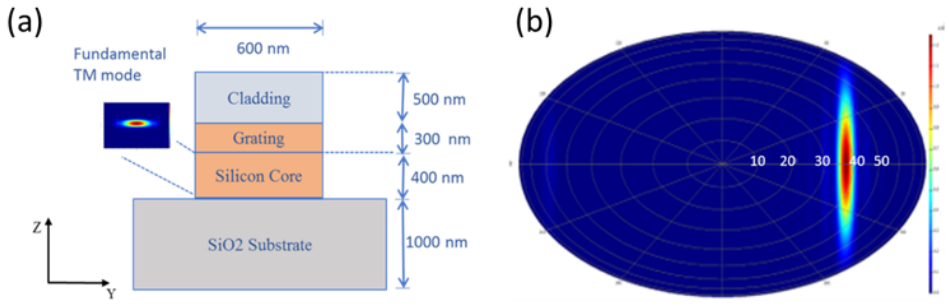

Figure 3.5: (a) Cross-sectional view of a single grating coupler (GC). (b) Simulated far-field radiation pattern of the GC, demonstrating the diffracted angle emitted from the GC ($\theta = 39°$), validating the expected theoretical value.The well-defined main lobe indicates efficient out-coupling of light into the desired direction.

3.4 2 channel Optical Phased Array

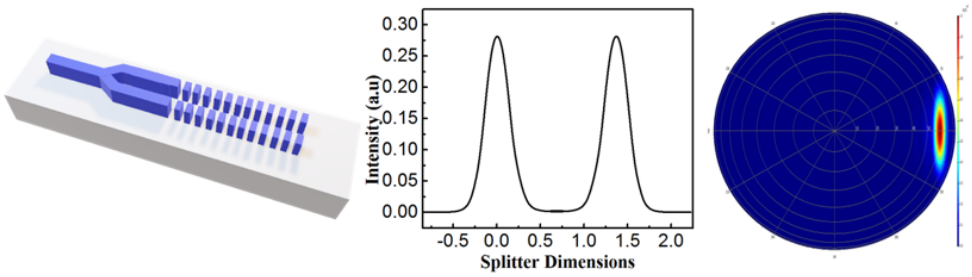

Figure 3.6: (a) 3D schematic view of a 2-channel optical phased array (OPA) with grating couplers separated by $\lambda/2$ (0.775 μm). (b) Optical intensity profile at the splitter output, demonstrating the power splitting between the two channels. (c) Far-field radiation pattern of the OPA, illustrating the combined beam intensity and directionality resulting from the interference of the two grating couplers.

The figure 3.6illustrates the design and performance of a 2-channel optical phased array (OPA) with grating couplers spaced at $\lambda/2$. The 3D schematic in (a) highlights the layout, while (b) reveals the power distribution at the splitter output, confirming balanced power delivery to both channels. The far-

field pattern in (c) demonstrates the constructive interference arising from the two grating couplers, resulting in a main beam directed at 60° with respect to the normal.

3.5 4 Channel Optical Phased Array

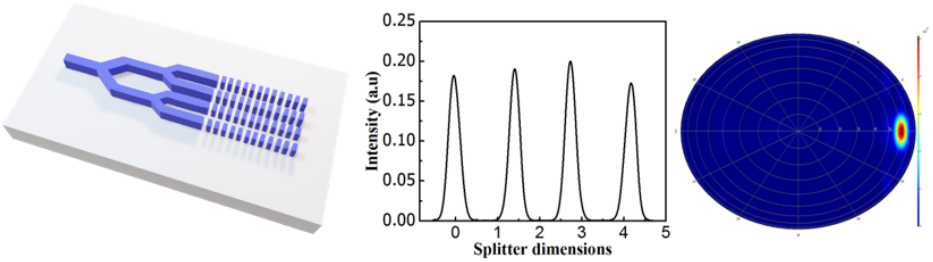

Figure 3.7: Design and Simulation of a 4-Channel Optical Phased Array (OPA) (a) 3D schematic illustrating the layout of a 4-channel OPA, featuring a splitter feeding four grating couplers arranged in a linear array. (b) Simulated optical intensity profile at the splitter output, showcasing power distribution among the four channels. (c) Far-field radiation pattern of the 4-channel OPA, demonstrating the combined beam resulting from the interference of light emitted from the four grating couplers.

The figure 3.7encapsulates the design and simulation results of a 4-channel optical phased array (OPA). The 3D schematic (a) reveals the OPA's architecture, consisting of a splitter and four grating couplers, each separated by $\lambda/2$ (0.775 μm)). The splitter output in (b) confirms a balanced power distribution across the four channels. The far-field radiation pattern in (c) highlights the constructive and destructive interference arising from the four grating couplers, leading to a specific beam profile similar in angle to a 2-channel OPA but with reduced beamwidth, indicative of increased directivity.

3.6 8 Channel Optical Phased Array

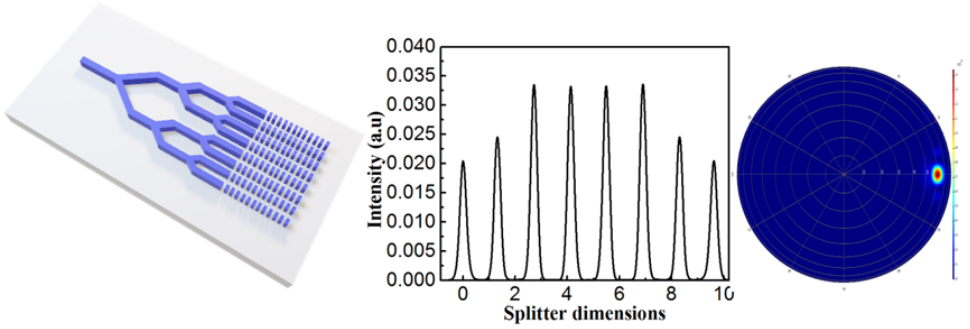

Figure 3.8: Design and Simulation of an 8-Channel Optical Phased Array (OPA)(a) 3D schematic illustrating the layout of an 8-channel OPA, featuring a cascading splitter tree feeding eight grating couplers arranged in a linear array.(b) Simulated optical intensity profile at the splitter output, showcasing the power distribution among the eight channels.(c) Far-field radiation pattern of the 8-channel OPA, demonstrating the combined beam resulting from the interference of light emitted from the eight grating couplers.

The figure 3.8encapsulates the design and simulation results of an 8-channel optical phased array (OPA). The 3D schematic (a) reveals the OPA's architecture, consisting of a cascading splitter tree that distributes the optical power to eight grating couplers. The splitter output in (b) confirms a relatively balanced power distribution across the eight channels, with slight variations due to the inherent nature of the splitter design. The far-field radiation pattern in (c) highlights the constructive and destructive interference arising from the eight grating couplers, leading to a specific beam profile with increased directivity compared to 2-channel and 4-channel OPAs.

3.7 16 Channel Optical Phased Array

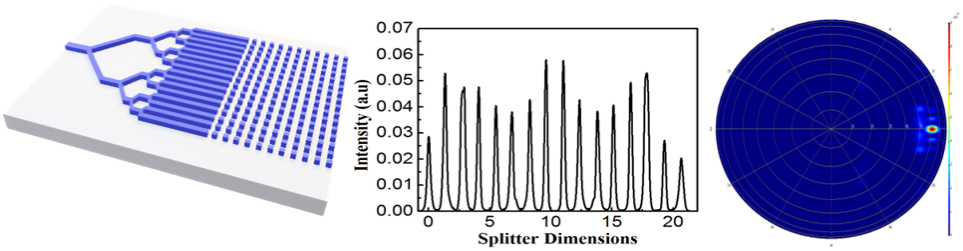

Figure 3.9: Design and Simulation of a 16-Channel Optical Phased Array (OPA)(a) 3D schematic illustrating the layout of a 16-channel OPA, featuring a cascading splitter tree feeding sixteen grating couplers arranged in a linear array.(b) Simulated optical intensity profile at the splitter output, showcasing the power distribution among the sixteen channels.(c) Far-field radiation pattern of the 16-channel OPA, demonstrating the combined beam resulting from the interference of light emitted from the sixteen grating couplers.

The figure 3.9 encapsulates the design and simulation results of a 16-channel optical phased array (OPA). The 3D schematic (a) reveals the OPA's architecture, consisting of a cascading splitter tree that distributes the optical power to sixteen grating couplers. The splitter output in (b) indicates a relatively balanced power distribution across the sixteen channels. The far-field radiation pattern in (c) displays a highly focused and directive beam due to the constructive interference of light from the numerous grating couplers. This configuration enables precise beam steering and shaping with enhanced resolution, making it ideal for applications like LiDAR that demand high accuracy and control over light emission

3.8 Results and Discussion

3.8.1 Lateral beam width of Proposed Design

Achieving high-resolution LIDAR demands minimizing the divergence of the output beam, a critical factor pivotal for precise sensing. The beam's divergence is significantly affected by the number of channels employed in the system, showing a direct relationship between these variables. In this pursuit,

aperture size plays a crucial role: as the aperture size increases, there's a simultaneous decrease in resolution. This inverse relationship between aperture size and resolution highlights the careful juggling required in designing LIDAR systems, where optimizing channel count while managing aperture dimensions becomes paramount. Balancing these elements is key to achieving optimal performance in LIDAR technology, ensuring both high resolution and minimized beam divergence crucial for accurate and detailed environmental mapping.Figure 3.10depicts the far field projections in Lumerical FDTD Solutions for the number of channels N = 2, N = 4, N = 8, N = 16. Figure 3.11depicts resolution of light getting better in lateral direction by increasing the number of channels from 2 to 16. The resolution ($\Delta_{\phi FWHM}$) of light is improved from 42 ° to 3.5 °

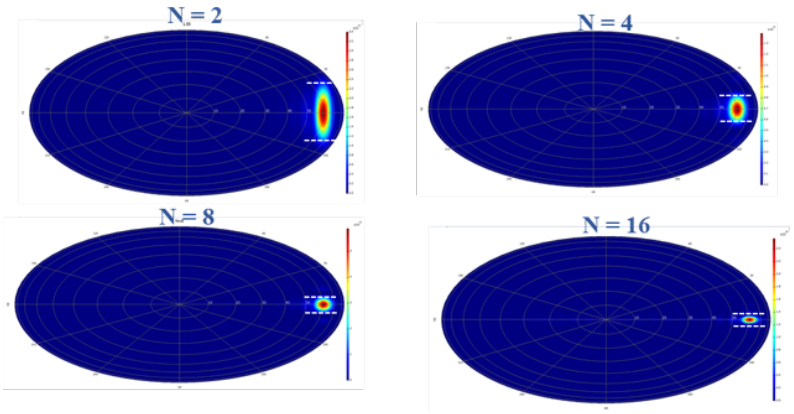

Figure 3.10: Variation in lateral beam width corresponding to the number of waveguides analyzed using FDTD Solutions

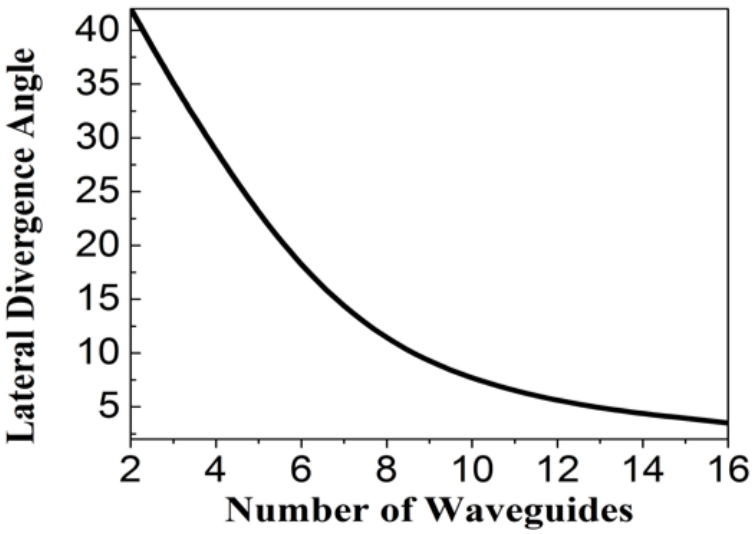

Figure 3.11: Relationship between beam divergence and the number of channels, emphasizing the dependency of divergence on the number of channels for a fixed channel spacing.

3.8.2 Lateral beam width of Proposed Design

The longitudinal beam width, quantifying the angular spread of the emitted beam along the longitudinal axis, exhibits analogous behavior to its lateral counterpart. In configurations where longitudinal beam steering is achieved through the coherent combination of multiple phased array elements, the beam width can be analytically derived using the same principles that govern the lateral beam width. However, alternative longitudinal steering mechanisms, such as wavelength tuning, introduce dependencies on factors such as the grating coupler design parameters (periodicity, fill factor), the overall grating length, and the specific operational wavelength. These dependencies necessitate a nuanced approach to beam width calculation and highlight the interplay between design parameters and operational choices in tailoring the angular dispersion of the OPA output.

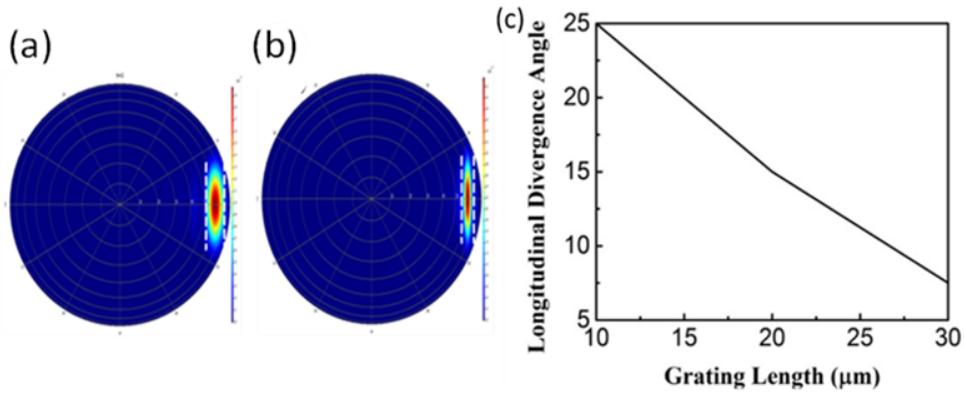

Figure 3.12: (a)-(b) Far field beam projections illustrating the beam's characteristics at grating lengths of 10 μm and 30 μm respectively.(c) Variation of Longitudinal divergence angle ($\Delta_{\theta FWHM}$) with respect to a grating length. As the length of the grating increases, there is a noticeable enhancement in beam resolution.

The Far field projection of the beam, depicted in Figure 3.12 (a)-(b) at grating lengths of 10 μm and 30 μm respectively, illustrates the substantial impact of varying grating lengths on the beam's spatial distribution. The comparison between these two far field projections highlight how altering the grating length significantly influences the divergence and directionality of the emitted beam. This data provides crucial insights into optimizing the device's performance and beam steering capabilities by manipulating the grating length within the system. Figure 3.12 depicts the beam's resolution noticeably improves from 25 ° to 7.5° along the Longitudinal direction with the increase in grating length from 10 μm to 30 μm. This extension directly enhances the precision of beam focusing. A longer grating significantly amplifies the capability to steer the beamresulting in a more distinct and defined resolution. This connection emphasizes the precisely controlling the beam's path along its length.

3.9 Longitudinal Steering of Proposed Design

The dynamic process of beam steering through wavelength modulation relies on a complex interplay between several key system parameters. Notably, the effective refractive index of the waveguide, the periodicity of the grating structure, the refractive index contrast between the waveguide and cladding, and the incident wavelength collectively govern the steering behavior. Adjust-

ing the wavelength enables precise control over the direction of the emitted beam. The effective refractive index of the waveguide dictates the light propagation path, while the grating pitch determines the diffraction angles and spectral dispersion. Moreover, the refractive index of the cladding influences the confinement and guiding of light within the waveguide. By carefully tuning these factors and leveraging wavelength modulation, a high degree of precision and accuracy can be achieved in steering the beam.Figure3.13 depicts the far field projections of a proposed design aimed at wavelength sweeping from 1.5 μm to 1.6 μm. These outcomes were obtained through the use of Lumerical Finite-difference time-domain (FDTD) solvers.

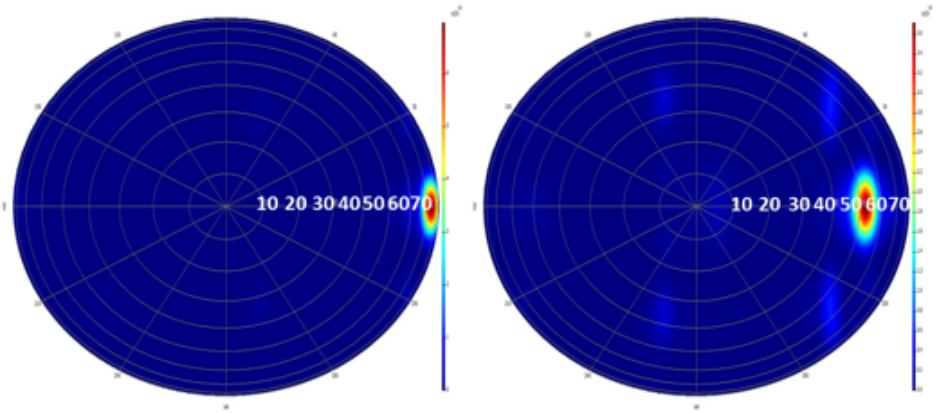

Figure 3.13: Far field projection of proposed device at 1.5 μm and 1.6 μm respectively. The Longitudinal angle (θ max) at 1.5 μm is 78 ° and at 1.6 μm is 55 °.

3.9.1 Lateral Steering of Proposed Design

The lateral steering angle (ϕ) is controlled by the phase delay (ϕ) between light injections in each grating coupler (GC). Beam steering is achieved by manipulating the phase shift, which is primarily done by adjusting the refractive index of the silicon waveguide. This alters the velocity of light propagation within the waveguide and, consequently, the phase delay between adjacent GCs.Electro-optic phase shifters are active photonic components that utilize the electro-optic effect to modify the phase of transmitted light.This phenomenon causes an applied electric field to alter the refractive index of the propagation medium. Precise control over the optical phase shift is achieved by modulating the applied electric field strength.Silicon-based optical mod-

ulators face challenges due to silicon's inherent limitations in electro-optic and thermo-optic effects, as well as weak light-matter interaction. These factors lead to large device footprints, high driving voltages, excessive energy consumption, and low extinction ratios. Current Si-based modulators are typically several millimeters in length, hindering compact integration. These challenges have prompted extensive research efforts aimed at developing novel approaches to mitigate these drawbacks. Miniaturizing modulators is a critical factor in enhancing on-chip packaging density and overall system integration.To overcome these limitations,silicon photonics is emerging as a promising solution. This approach combines device engineering with material engineering. Device engineering focuses on innovative photonic device designs for enhanced light-matter interaction, while material engineering involves integrating low-cost, tunable materials with silicon.

Indium tin oxide (ITO) has emerged as a compelling material for this purpose. It exhibits rapid carrier dynamics and substantial carrier accumulation/depletion,resulting in significant bias-dependent absorption changes. Additionally, ITO's permittivity (and thus refractive index) undergoes a significant shift. Notably, ITO can be electrically configured to approach the epsilon-near-zero (ENZ) state in the near-infrared region, leading to an abrupt change in absorption and enabling efficient optical modulation. The Far Field Projections depicted in Fig.3.14 showcase the distinct performance of two electro-optic phase shifters within the proposed device. In figure (a), employing Si as the phase shifter reveals a notable observation: despite the application of voltage across the Si phase shifter, no lateral steering is observed. This absence of lateral steering prompts further examination of Si's functionality within the device. Notably, due to the weak electro-optic properties of silicon, a considerable voltage and substantialdevice footprint are required to induce a change in refractive index and subsequently alter the phase. Conversely, in figure (b) presents a significant contrast, featuring Si-ITO as the electro-optic phase shifter. Here, the application of a mere 1-volt voltage leads to a noticeable and promising lateral steering effect. This marked difference in behavior is attributed to Si-ITO's superior electro-optic effect, enabling rapid changes in refractive index under bias conditions. The clear distinction in lateral steering behavior between the two materials Si and Si-ITO highlights the crucial role of material properties in achieving efficient electro-optic phase shifting within the device. The Far Field Projections seen in Fig. (c)-(d) highlight the impressive abilities of the proposed Si-ITO phase shifter device. In this part of the figure, applying 1 volt selectively to the bottom 8 phase shifters directs the beam at +28°, while the same voltage applied to the top 8 phase shifters positions the beam at -28°. This clear difference in beam angles re-

sults in a substantial 56° range, representing the maximum lateral steering achieved by this setup. This precise control over beam direction showcases the adaptability enabled by Si-ITO phase shifters, offering significant potential for applications requiring precise beam manipulation

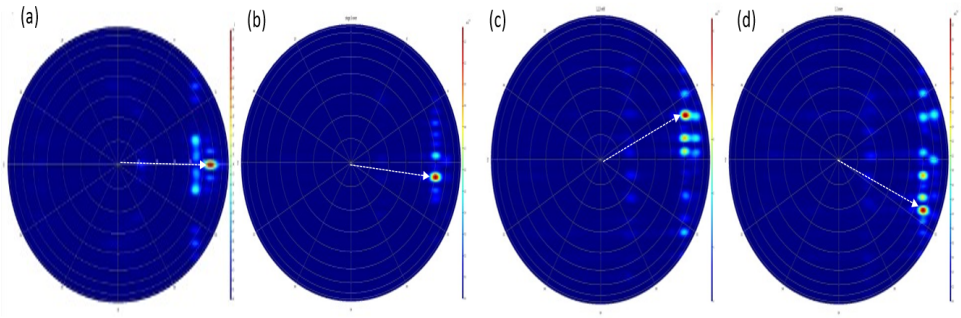

Figure 3.14: Far Field Projections illustrating lateral steering behavior: (a) Device utilizing Si as an electro-optic phase shifter of same dimensions shows no lateral steering despite applied voltage; (b) Si-ITO as an electro-optic phase shifter demonstrates effective lateral steering at 1 volt at 15th and 16th phase shifters, (c)-(d) Far Field Projections of the proposed device employing Si-ITO phase shifters. In subfigure (c), notable beam steering capabilities are showcased. Specifically, applying 1 volt to the bottom 8 phase shifters (1-8) results in a beam angle of +28°, In subfigure (d) the top 8 phase shifters (9-16), under the same voltage, produce a beam angle of -28°. This distinct configuration achieves a substantial 56° range, highlighting the precise control achieved through specific phase shifts within the device.

This extensive range highlights the efficacy and versatility of employing Si-ITO phase shifters in dynamically controlling the beam direction, emphasizing the device's capacity for agile and precise beam steering functionalities across a broad angular spectrum. Such findings underscore the considerable potential for practical applications in optical systems requiring adaptable and extensive beam manipulation for various functionalities and scenarios.

3.10 Summary

In this study, a 16-channel optical phased array (OPA) was systematically constructed, simulated in MODE and FDTD Solutions. The process began with the design and optimization of a single grating coupler, analyzing the impact of various design parameters. Subsequently, a 2-channel OPA was realized by

optimizing a 1x2 splitter. This approach was iteratively expanded, creating 4, 8, and 16-channel OPAs with corresponding 1x4, 1x8, and 1x16 Y splitters. Far-field simulations were conducted to assess performance, and both lateral and longitudinal divergence angles were calculated. Wavelength sweeps from 1.5 to 1.6 μm facilitated longitudinal steering, while the implementation of Si-ITO phase shifters enabled lateral steering capabilities of up to 56°.

Chapter 4

Conclusion and Future Scope

This study employed a comprehensive simulation-based approach to investigate the design and optimization of silicon photonics-based optical phased arrays (OPAs) for beam steering applications, focusing on the optimization of grating couplers and array configurations. FDTD simulations were employed to analyze far-field radiation patterns, revealing the influence of grating pitch and duty cycle on beam characteristics. For single grating couplers, smaller grating pitches enabled wider steering angles but compromised coupling efficiency, while larger pitches enhanced efficiency but limited steering range. The emergence of grating lobes when the pitch exceeded half the wavelength emphasized the need for careful design considerations. Duty cycle analysis highlighted a trade-off between main lobe width and side lobe intensity, with 0.5 identified as optimal for focused beam steering.The study then extended to multi-channel OPAs, demonstrating a scalable design approach from 2 to 16 channels using cascading splitters, with a final device footprint of 0.07 mm x 0.02 mm. This compact size is a significant advantage compared to previous work, such as the 1 mm x 9 mm device by Kwong et al. (2014) and the 1200 μm x 200 μm device by Poulton et al. (2016). Results showed that increasing channel count improved beam directivity, reduced beam width, and facilitated precise beam steering. A maximum lateral steering angle of 56° was achieved using Si-ITO phase shifters, surpassing the 20° achieved by Kwong et al. (2014) and comparable to the 46° achieved by Poulton et al. (2016). Longitudinal steering was realized through wavelength tuning from 1.5 μm to 1.6 μm, yielding steering angles from 55° to 78°. Furthermore, the effects of grating length on longitudinal beam divergence were explored, revealing improved resolution with longer gratings.The utilization of Si-ITO phase shifters in our design offers a significant advantage in terms of device compactness compared to traditional silicon-based phase shifters, which require larger footprints to achieve comparable steering performance. The su-

perior electro-optic properties of Si-ITO enable efficient phase control within a reduced area, contributing to the overall miniaturization of the OPA system.In conclusion, this comprehensive simulation-based study provides a detailed understanding of the impact of design parameters on the performance of compact, multi-channel OPAs for precise and versatile beam steering in applications such as LiDAR. By thoroughly exploring the effects of various parameters and demonstrating a scalable design methodology, our findings pave the way for the development of high-performance OPAs with improved miniaturization and steering capabilities.

Optical phased arrays (OPAs) have emerged as a promising technology for solid-state beam steering, poised to replace traditional mechanical methods due to their inherent advantages in size, weight, and power consumption. While OPAs offer numerous advantages for applications like LIDAR, achieving a wide steering range, high angular resolution, and low power consumption simultaneously remains a central focus of ongoing research.

As research in this domain progresses, it is anticipated that OPAs will become increasingly sophisticated and versatile, capable of dynamic beam shaping and steering for a wider array of applications across diverse fields. These advancements could revolutionize technologies such as autonomous vehicles, robotics, free-space optical communications, and biomedical imaging in a new era of optical beam steering capabilities.

Bibliography

[1] M. U. Khan, Y. Xing, Y. Ye, and W. Bogaerts, "Photonic integrated circuit design in a foundry+fabless ecosystem," *IEEE Journal of Selected Topics in Quantum Electronics*, vol. 25, no. 5, pp. 1–14, 2019. DOI: 10.1109/JSTQE.2019.2918949.

[2] S. Siew, B. Li, G. Feng, *et al.*, "Review of silicon photonics technology and platform development," *Journal of Lightwave Technology*, vol. PP, pp. 1–1, Mar. 2021. DOI: 10.1109/JLT.2021.3066203.

[3] E. Pelucchi, G. Fagas, I. Aharonovich, *et al.*, "The potential and global outlook of integrated photonics for quantum technologies," *Nature Reviews Physics*, vol. 4, Dec. 2021. DOI: 10.1038/s42254-021-00398-z.

[4] C.-P. Hsu, B. Li, B. Solano-Rivas, *et al.*, "A review and perspective on optical phased array for automotive lidar," *IEEE Journal of Selected Topics in Quantum Electronics*, vol. 27, no. 1, pp. 1–16, 2021. DOI: 10.1109/JSTQE.2020.3022948.

[5] M. Jaboyedoff, T. Oppikofer, A. Abellán, *et al.*, "Use of lidar in landslide investigations: A review," *Natural hazards*, vol. 61, pp. 5–28, 2012.

[6] S. Chung, H. Abediasl, and H. Hashemi, "A monolithically integrated large-scale optical phased array in silicon-on-insulator cmos," *IEEE Journal of Solid-State Circuits*, vol. 53, no. 1, pp. 275–296, 2018. DOI: 10.1109/JSSC.2017.2757009.

[7] K. V. Acoleyen, H. Rogier, and R. Baets, "Two-dimensional optical phased array antenna on silicon-on-insulator," *Opt. Express*, vol. 18, no. 13, pp. 13 655–13 660, Jun. 2010. DOI: 10.1364/OE.18.013655. [Online]. Available: https://opg.optica.org/oe/abstract.cfm?URI=oe-18-13-13655.

[8] H. Abediasl and H. Hashemi, "Monolithic optical phased-array transceiver in a standard soi cmos process," *Opt. Express*, vol. 23, no. 5, pp. 6509–6519, Mar. 2015. DOI: 10.1364/OE.23.006509. [Online]. Available: https://opg.optica.org/oe/abstract.cfm?URI=oe-23-5-6509.

[9] B. Smith, B. Hellman, A. Gin, A. Espinoza, and Y. Takashima, "Single chip lidar with discrete beam steering by digital micromirror device," *Opt. Express*, vol. 25, no. 13, pp. 14 732–14 745, Jun. 2017. DOI: 10.1364/OE.25.014732. [Online]. Available: https://opg.optica.org/oe/abstract.cfm?URI=oe-25-13-14732.

[10] K. V. Acoleyen, W. Bogaerts, J. Jágerská, N. L. Thomas, R. Houdré, and R. Baets, "Off-chip beam steering with a one-dimensional optical phased array on silicon-on-insulator," *Opt. Lett.*, vol. 34, no. 9, pp. 1477–1479, May 2009. DOI: 10.1364/OL.34.001477. [Online]. Available: https://opg.optica.org/ol/abstract.cfm?URI=ol-34-9-1477.

[11] T. Chan, M. Megens, B.-W. Yoo, *et al.*, "Optical beamsteering using an 8 × 8 mems phased array with closed-loop interferometric phase control," *Optics Express*, vol. 21, pp. 2807–2815, Jan. 2013. DOI: 10.1364/OE.21.002807.

[12] A. Yaacobi, J. Sun, M. Moresco, G. Leake, D. Coolbaugh, and M. Watts, "Integrated phased array for wide-angle beam steering," *Optics Letters*, vol. 39, Jul. 2014. DOI: 10.1364/OL.39.004575.

[13] D. R. Gozzard, L. E. Roberts, J. T. Spollard, P. G. Sibley, and D. A. Shaddock, "Fast beam steering with an optical phased array," *Opt. Lett.*, vol. 45, no. 13, pp. 3793–3796, Jul. 2020. DOI: 10.1364/OL.393007. [Online]. Available: https://opg.optica.org/ol/abstract.cfm?URI=ol-45-13-3793.

[14] Y. Liu and H. Hu, "Silicon optical phased array with a 180-degree field of view for 2d optical beam steering," *Optica*, vol. 9, no. 8, pp. 903–907, Aug. 2022. DOI: 10.1364/OPTICA.458642. [Online]. Available: https://opg.optica.org/optica/abstract.cfm?URI=optica-9-8-903.

[15] J. Van Campenhout, W. Green, S. Assefa, and Y. Vlasov, "Integrated nisi waveguide heaters for cmos-compatible silicon thermo-optic devices," *Optics letters*, vol. 35, pp. 1013–5, Apr. 2010. DOI: 10.1364/OL.35.001013.

[16] A. Masood, M. Pantouvaki, D. Goossens, *et al.*, "Fabrication and characterization of cmos-compatible integrated tungsten heaters for thermo-optic tuning in silicon photonics devices," *Optical Materials Express*, vol. 4, p. 1383, Jun. 2014. DOI: 10.1364/OME.4.001383.

[17] C. Barrios and M. Lipson, "Modeling and analysis of high-speed electro-optic modulation in high confinement silicon waveguides using metal-oxide-semiconductor configuration," *Journal of Applied Physics*, vol. 96, pp. 6008–6015, Jan. 2005. DOI: 10.1063/1.1814791.

[18] C. V. Poulton, P. Russo, E. Timurdogan, *et al.*, "High-performance integrated optical phased arrays for chip-scale beam steering and lidar," in *Conference on Lasers and Electro-Optics*, Optica Publishing Group, 2018, ATu3R.2. DOI: 10.1364/CLEO_AT.2018.ATu3R.2. [Online]. Available: https://opg.optica.org/abstract.cfm?URI=CLEO_AT-2018-ATu3R.2.

[19] C.-S. Im, B. Bhandari, K.-P. Lee, S.-M. Kim, M.-C. Oh, and S.-S. Lee, "Silicon nitride optical phased array based on a grating antenna enabling wavelength-tuned beam steering," *Opt. Express*, vol. 28, no. 3, pp. 3270–3279, Feb. 2020. DOI: 10.1364/OE.383304. [Online]. Available: https://opg.optica.org/oe/abstract.cfm?URI=oe-28-3-3270.

[20] C. Poulton, M. Byrd, M. Raval, *et al.*, "Large-scale silicon nitride nanophotonic phased arrays at infrared and visible wavelengths," *Optics Letters*, vol. 42, pp. 21–24, Dec. 2016. DOI: 10.1364/OL.42.000021.

[21] D. Moss, R. Morandotti, A. Gaeta, and M. Lipson, "New cmos-compatible platforms based on silicon nitride and hydex for nonlinear optics," *Nature Photonics*, vol. 7, pp. 597–607, Jul. 2013. DOI: 10.1038/nphoton.2013.183.

[22] L. Cheng, S. Mao, Z. Li, Y. Han, and H. Y. Fu, "Grating couplers on silicon photonics: Design principles, emerging trends and practical issues," *Micromachines*, vol. 11, no. 7, 2020, ISSN: 2072-666X. DOI: 10.3390/mi11070666. [Online]. Available: https://www.mdpi.com/2072-666X/11/7/666.

[23] P. A. Krochin Yepez, U. Scholz, and A. Zimmermann, "Cmos-compatible measures for thermal management of phase-sensitive silicon photonic systems," *Photonics*, vol. 7, p. 6, Jan. 2020. DOI: 10.3390/photonics7010006.

[24] Y. Wang, L. Liang, Y. Chen, *et al.*, "Improved performance of optical phased arrays assisted by transparent graphene nanoheaters and air trenches," *RSC Advances*, vol. 8, pp. 8442–8449, Feb. 2018. DOI: 10.1039/C7RA13154B.

[25] L. Yu, L. Liu, Z. Zhou, and X. Wang, "High efficiency binary blazed grating coupler for perfectly-vertical and near-vertical coupling in chip level optical interconnections," *Optics Communications*, vol. 355, Nov. 2015. DOI: 10.1016/j.optcom.2015.06.003.

[26] Y. Wang, "Grating coupler design based on silicon-on-insulator," Ph.D. dissertation, University of British Columbia, 2013. DOI: http://dx.doi.org/10.14288/1.0073806. [Online]. Available: https://open.library.ubc.ca/collections/ubctheses/24/items/1.0073806.

[27] G. Roelkens, D. Thourhout, and R. Baets, "High efficiency grating coupler between silicon-on-insulator waveguides and perfectly vertical optical fibers," *Optics letters*, vol. 32, pp. 1495–7, Jul. 2007. DOI: 10.1364/OL.32.001495.

[28] D. Benedikovič, C. Alonso-Ramos, D. Perez-Galacho, *et al.*, "L-shaped fiber-chip grating couplers with high directionality and low reflectivity fabricated with deep-uv lithography," *Optics Letters*, vol. 42, p. 3439, Aug. 2017. DOI: 10.1364/OL.42.003439.

[29] G. Roelkens, D. V. Thourhout, and R. Baets, "High efficiency grating coupler between silicon-on-insulator waveguides and perfectly vertical optical fibers," *Opt. Lett.*, vol. 32, no. 11, pp. 1495–1497, Jun. 2007. DOI: 10.1364/OL.32.001495. [Online]. Available: https://opg.optica.org/ol/abstract.cfm?URI=ol-32-11-1495.

[30] L. Liu, J. Zhang, C. Zhang, *et al.*, "Silicon waveguide grating coupler for perfectly vertical fiber based on a tilted membrane structure," *Optics Letters*, vol. 41, p. 820, Feb. 2016. DOI: 10.1364/OL.41.000820.

[31] M. Jacques, A. Samani, E. El-Fiky, D. Patel, Z. Xing, and D. V. Plant, "Optimization of thermo-optic phase-shifter design and mitigation of thermal crosstalk on the soi platform," *Opt. Express*, vol. 27, no. 8, pp. 10 456–10 471, Apr. 2019. DOI: 10.1364/OE.27.010456. [Online]. Available: https://opg.optica.org/oe/abstract.cfm?URI=oe-27-8-10456.

[32] S. Yan, X. Zhu, L. Frandsen, *et al.*, "Slow-light-enhanced energy efficiency for the graphene microheater on silicon photonic crystal waveguides," *Nature Communications*, vol. 8, p. 14 411, Feb. 2017. DOI: 10.1038/ncomms14411.

[33] H. Qiu, Y. Liu, C. Luan, *et al.*, "Energy-efficient thermo-optic silicon phase shifter with well-balanced overall performance," *Optics Letters*, vol. 45, Aug. 2020. DOI: 10.1364/OL.400230.

[34] M. Jacques, A. Samani, E. El-Fiky, D. Patel, Z. Xing, and D. Plant, "Optimization of thermo-optic phase-shifter design and mitigation of thermal crosstalk on the soi platform," *Optics Express*, vol. 27, pp. 10 456–10 471, Apr. 2019. DOI: 10.1364/OE.27.010456.

[35] H. Sun, Q. Qiao, Q. Guan, and G. Zhou, "Silicon photonic phase shifters and their applications: A review," *Micromachines*, vol. 13, no. 9, 2022, ISSN: 2072-666X. DOI: 10.3390/mi13091509. [Online]. Available: https://www.mdpi.com/2072-666X/13/9/1509.

[36] Y. Kim, M. Takenaka, and S. Takagi, "Numerical analysis of carrier-depletion strained sige optical modulators with vertical p-n junction," *IEEE Journal of Quantum Electronics*, vol. 51, no. 4, pp. 1–7, 2015. DOI: 10.1109/JQE.2015.2405931.

[37] Y. Kim, M. Takenaka, T. Osada, M. Hata, and S. Takagi, "Strain-induced enhancement of plasma dispersion effect and free-carrier absorption in sige optical modulators," *Scientific reports*, vol. 4, p. 4683, Apr. 2014. DOI: 10.1038/srep04683.

[38] M. Takenaka and S. Takagi, "Strain engineering of plasma dispersion effect for sige optical modulators," *IEEE Journal of Quantum Electronics - IEEE J QUANTUM ELECTRON*, vol. 48, pp. 8–16, Jan. 2012. DOI: 10.1109/JQE.2011.2176104.

[39] T. Hu, H. Qiu, Z. Zhang, *et al.*, "A compact ultrabroadband polarization beam splitter utilizing a hybrid plasmonic y-branch," *IEEE Photonics Journal*, vol. 8, pp. 1–1, Aug. 2016. DOI: 10.1109/JPHOT.2016.2585113.

[40] G. Huang, T.-H. Park, and M.-C. Oh, "Broadband integrated optic polarization splitters by incorporating polarization mode extracting waveguide," *Scientific Reports*, vol. 7, Jul. 2017. DOI: 10.1038/s41598-017-05324-x.

[41] W. Guo, P. R. A. Binetti, C. Althouse, *et al.*, "Two-dimensional optical beam steering with inp-based photonic integrated circuits," *IEEE Journal of Selected Topics in Quantum Electronics*, vol. 19, no. 4, pp. 6 100 212–6 100 212, 2013. DOI: 10.1109/JSTQE.2013.2238218.

[42] D. Kwong, A. Hosseini, J. Covey, *et al.*, "On-chip silicon optical phased array for two-dimensional beam steering," *Opt. Lett.*, vol. 39, no. 4, pp. 941–944, Feb. 2014. DOI: 10.1364/OL.39.000941. [Online]. Available: https://opg.optica.org/ol/abstract.cfm?URI=ol-39-4-941.

[43] J. C. Hulme, J. K. Doylend, M. J. R. Heck, *et al.*, "Fully integrated hybrid silicon two dimensional beam scanner," *Opt. Express*, vol. 23, no. 5, pp. 5861–5874, Mar. 2015. DOI: 10.1364/OE.23.005861. [Online]. Available: https://opg.optica.org/oe/abstract.cfm?URI=oe-23-5-5861.

[44] C. V. Poulton, A. Yaacobi, Z. Su, M. J. Byrd, and M. R. Watts, "Optical phased array with small spot size, high steering range and grouped cascaded phase shifters," in *Advanced Photonics 2016 (IPR, NOMA, Sensors, Networks, SPPCom, SOF)*, Optica Publishing Group, 2016, IW1B.2. DOI: 10.1364/IPRSN.2016.IW1B.2. [Online]. Available: https://opg.optica.org/abstract.cfm?URI=IPRSN-2016-IW1B.2.

[45] D. N. Hutchison, J. Sun, J. K. Doylend, *et al.*, "High-resolution aliasing-free optical beam steering," *Optica*, vol. 3, no. 8, pp. 887–890, Aug. 2016. DOI: 10.1364/OPTICA.3.000887. [Online]. Available: https://opg.optica.org/optica/abstract.cfm?URI=optica-3-8-887.

[46] Y. Li, B. Chen, Q. Na, *et al.*, "Wide-steering-angle high-resolution optical phased array," *Photon. Res.*, vol. 9, no. 12, pp. 2511–2518, Dec. 2021. DOI: 10.1364/PRJ.437846. [Online]. Available: https://opg.optica.org/prj/abstract.cfm?URI=prj-9-12-2511.

[47] S. Rajput, V. Kaushik, L. Singh, S. S. K. Pandey, R. D. Mishra, and M. Kumar, "Efficient photodetector based on sub-bandgap transition in silicon-ito distributed-heterojunctions," *Journal of Lightwave Technology*, vol. 39, no. 21, pp. 6886–6892, 2021. DOI: 10.1109/JLT.2021.3106451.

[48] S. Rajput, V. Kaushik, P. Babu, P. Tiwari, A. Srivastava, and M. Kumar, "Optical modulation via coupling of distributed semiconductor heterojunctions in a si -ito-based subwavelength grating," *Physical Review*

Applied, vol. 15, pp. 054 029–1, Apr. 2021. DOI: 10.1103/PhysRevApplied.15.054029.

[49] S. Rajput, V. Kaushik, P. Babu, S. Pandey, and M. Kumar, "All optical modulation in vertically coupled indium tin oxide ring resonator employing epsilon near zero state," *Scientific Reports*, vol. 13, Oct. 2023. DOI: 10.1038/s41598-023-44438-3.